

Revisiting a Receptor-Based Pharmacophore Hypothesis for Human A_{2A} Adenosine Receptor Antagonists

Magdalena Bacilieri,^{†,▽} Antonella Cincetta,^{†,▽} Silvia Paoletta,[†] Stephanie Federico,[‡] Sandro Cosconati,[§] Barbara Cacciarri,^{||} Sabrina Taliani,[⊥] Federico Da Settimo,[⊥] Ettore Novellino,[§] Karl Norbert Klotz,[#] Giampiero Spalluto,[‡] and Stefano Moro^{*,†}

[†]Molecular Modeling Section (MMS), Dipartimento di Scienze del Farmaco, Università di Padova, via Marzolo 5, Padova, Italy

[‡]Dipartimento di Scienze Chimiche e Farmaceutiche, Università di Trieste, Piazzale Europa 1, Trieste, Italy

[§]Dipartimento di Chimica Farmaceutica e Tossicologica, Università "Federico II", Via Montesano 49, 80131 Napoli, Italy

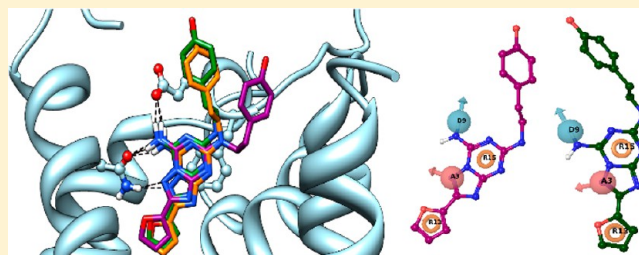
^{||}Dipartimento di Scienze Farmaceutiche, Università degli Studi di Ferrara, via Fossato di Mortara 17-19, 44100 Ferrara, Italy

[⊥]Dipartimento di Scienze Farmaceutiche, Università di Pisa, Via Bonanno 6, 56126 Pisa, Italy

[#]Institut für Pharmakologie, Universität of Würzburg, D-97078 Würzburg, Germany

Supporting Information

ABSTRACT: The application of both structure- and ligand-based design approaches represents to date one of the most useful strategies in the discovery of new drug candidates. In the present paper, we investigated how the application of docking-driven conformational analysis can improve the predictive ability of 3D-QSAR statistical models. With the use of the crystallographic structure in complex with the high affinity antagonist ZM 241385 (4-(2-[7-amino-2-(2-furyl)[1,2,4]-triazolo[2,3-a][1,3,5]triazin-5-ylamino]ethyl)phenol), we revisited a general pharmacophore hypothesis for the human A_{2A} adenosine receptor of a set of 751 known antagonists, by applying an integrated ligand- and structure-based approach. Our novel pharmacophore hypothesis has been validated by using an external test set of 29 newly synthesized human adenosine receptor antagonists.



■ INTRODUCTION

Adenosine is a neuromodulator whose biological functions are accomplished through the activation of specific proteins belonging to the G protein-coupled receptors (GPCRs) superfamily. To date, four distinct Adenosine Receptor (AR) subtypes, termed A₁, A_{2A}, A_{2B}, and A₃, have been identified and classified according to pharmacological criteria and activation or inhibition of adenylyl cyclase activity.^{1–3}

Owing to the wide range of effects exerted in numerous organ systems, the activation or blockade of ARs finds potential therapeutic applications in the treatment of several pathologies, such as cardiac and cerebral ischemia, asthma, Parkinson's disease, cancer, and kidney diseases.^{4–10} In view of their potential application for pharmaceutical purposes, several groups have focused their attention on the synthesis of both AR agonists and antagonists, especially aimed by the pharmacological and biophysical characterization of the receptors.^{11,12} In the field of AR antagonist development, several classes of compounds with a broad range of affinities and selectivities have emerged. In particular, heterocycles such as pyrazolo-triazolo-pyrimidines (PTP), xanthines, adenines, triazolopyrazines, and triazolotriazines have been identified as suitable scaffolds.^{13–18}

Notably, over the past 20 years, the development of new classes of AR antagonists has been supported by computational

techniques aimed at exploring structure–activity relationships and providing clues on the most promising functionalizations of the emerged scaffolds. As long as no structural information about ARs has been available, the computational efforts have been mainly devoted to the development of three-dimensional Quantitative Structure–Activity Relationship (3D-QSAR) predictive models.^{19–23} In fact, structure-based approaches have been confined to homology models,^{24–27} whose application has been hampered by the low sequence homology between the available bovine rhodopsin crystal structures and ARs. Consequently, their use has been mainly directed toward the retrospective analysis of the binding of known structures rather than for structure-based drug design.

The disclosure of the crystal structure of the human A_{2A} AR in complex with both agonists and antagonists^{28–34} has allowed structure-based design approaches to take a step forward and opened up the possibility to test and develop combined structure- and ligand-based strategies also for this class of receptors. This integrated approach, indeed, has been recently successfully applied to another class of GPCRs.³⁵

Received: October 8, 2012

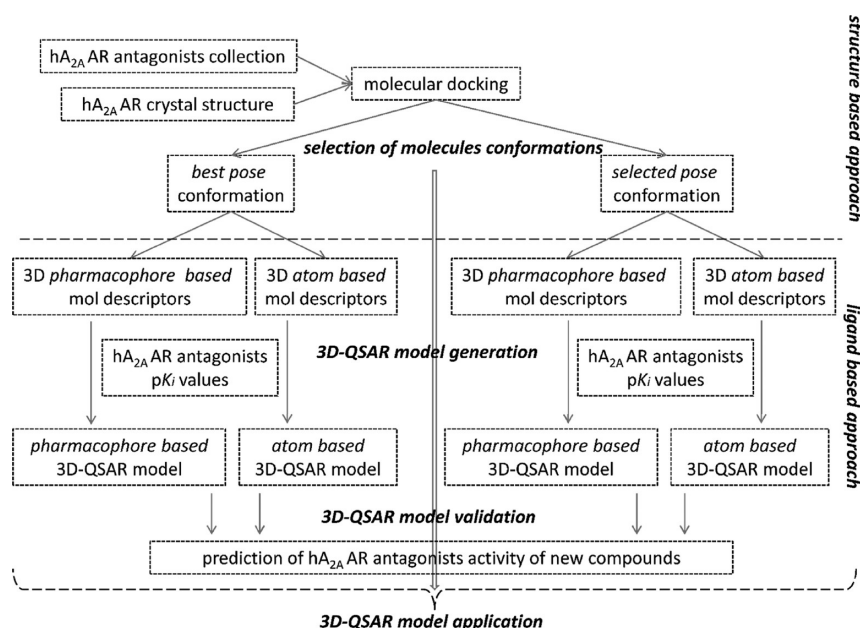


Figure 1. Flowchart of the Integrated Ligand- and Structure-Based Approach.

The underlying idea of a combined strategy is to increase the success of the *in silico* drug discovery processes by merging the strengths of the two approaches. On one hand, a structure-based approach such as molecular docking can “exhaustively” explore the conformational space of a ligand inside its binding cavity, by inferring on the possible ligand “bioactive” conformation; on the other hand, ligand-based approaches are able to correlate and predict biological activities on the basis of molecular properties (molecular descriptors).^{36,37} Moreover, the integrated approach aims also at overcoming some of the known drawbacks of each merged technique, such as for example the lack of robust scoring functions for the estimate of ligand-target binding affinities in the case of molecular docking²⁷ and the need for the availability of bioactive conformations, as required by 3D-QSAR approaches, such as Comparative Molecular Field Analysis (CoMFA) or 3D-pharmacophore search. Therefore, the use of conformations generated by molecular docking simulations might represent the natural “structural” input of a conventional 3D-QSAR study in all those cases when no experimental information about the “bioactive” conformer is available or any structural superimposition protocol, required for CoMFA, is not achievable.^{27,38–40}

The aim of the present study has been therefore to explore whether the application of docking-driven conformational analysis increases the quality of 3D-QSAR statistical models, by selecting as a key study an ensemble of human A_{2A} AR antagonists. For this purpose, we have collected a database of 751 compounds comprising all major chemical classes of human A_{2A} AR antagonists actually discovered, which currently represents one of the largest molecular collections used to generate a quantitative model for the hA_{2A} AR antagonists.^{21,41–80} All 751 compounds have been subjected to molecular docking simulations at the hA_{2A} AR, and from the resulting conformations two data sets have been derived: one comprising the best poses as defined by the docking scoring function and another one consisting of poses selected through visual inspection by considering crucial interactions between the ligands and the binding site residues as emerged by the available crystal structures. For both sets, both 3D *pharmacophore*- and *atom-based* molecular descriptors have been computed and then processed to develop *pharmacophore*- and *atom-based* 3D-QSAR

models. As our group has extensively investigated the PTP nucleus for AR antagonists,^{21,27,49,80–82} the models have been validated using an external test set of 29 new PTP compounds. The flowchart of the work is reported in Figure 1.

MATERIALS AND METHODS

Computational Methodologies. Docking simulations were performed using the GOLD suite (version 5.1).⁸³ Energy calculation and analyses of docking poses were performed using the Molecular Operating Environment (MOE, version 2010.10) suite.⁸⁴ Quantum mechanical calculations were carried out with the software package MOPAC (version 7), as implemented in the MOE suite.

Pharmacophore hypotheses and 3D-QSAR models were generated with the PHASE module⁸⁵ of the Schrödinger Suite 2010.⁸⁶

For all of the above-mentioned software packages, we used the default settings, unless otherwise specified (non-default parameters are reported in brackets).

Molecular Database. A database of 751 hA_{2A} AR antagonists has been collected from recent literature: In particular, we selected all known hA_{2A} AR antagonists showing $K_i < 1 \mu\text{M}$ ($\text{p}K_i > -3$), with the K_i values measured through the displacement of selective radioligands.^{21,41–80} The 751 compounds can be grouped into 22 different scaffolds (see Figure 2), and their corresponding structures and pharmacological binding data are collected in the Supporting Information.

In each analysis, the compounds have been split into a training and a test database: 80% has been randomly selected as the training set and 20% as the test set.

Moreover, a new small antagonist library has also been synthesized and pharmacologically characterized: The new external test set comprises 29 PTP compounds, whose structures and pharmacological profiles at the hA_{2A} AR are reported in Table 1.

Three-Dimensional Structure of hA_{2A} AR. Among all the available crystallographic structures of the hA_{2A} AR, we selected for our docking simulations the complex with the high affinity antagonist ZM 241385 (PDB code: 3EML).²⁸ As it is conceivable

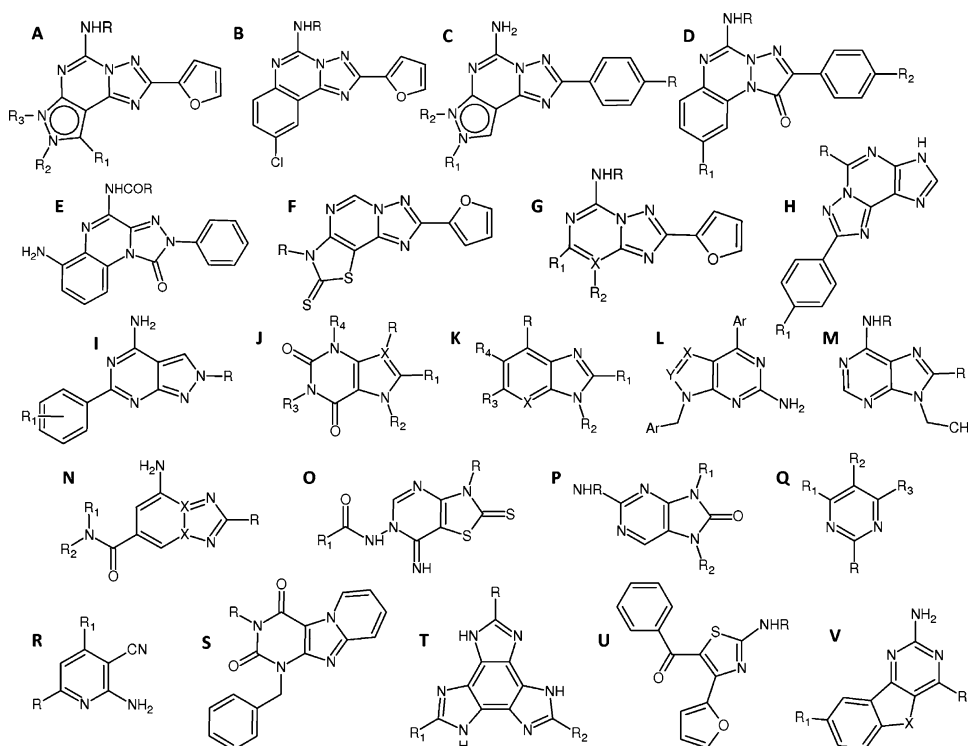


Figure 2. Molecular scaffolds referring to the 751 selected hA_{2A} AR antagonists.

to expect that compounds sharing structural similarity might interact similarly with the receptor subtype, our choice has been driven by the higher structural similarity that the 22 different scaffolds share with ZM 241385 with respect to the other cocrystallized antagonists. We quantified such similarity through a combined consensus shape- and pharmacophore-based similarity index as implemented in the “Best Template Searching” option in our Adenosiland platform (<http://mms.dsfarm.unipd.it/Adenosiland/>).⁸⁷ The search has been conducted for the most active compounds for each scaffold, which are reported in Table S1 (cocrystallized ligands are reported with the three letters code assigned to them in the corresponding PDB file): ZM 241385 (ZMA) is the antagonist most similar to the scaffolds represented in the database. Moreover, we also quantified the number of compounds in the whole database similar to all the cocrystallized antagonists: For that purpose, we performed a similarity search based on MACCS fingerprints and the Tanimoto metric as implemented in MOE⁸⁴ by setting different overlap values ranging from 45% to 80% (see Table S2). In all cases, ZM 241385 is the antagonist most structurally similar to the majority of compounds in the database.

At the time we performed this study, there were four crystallographic complexes with ZM 241385 (3EML,²⁸ 3PWH,³¹ 3VG9, and 3VGA³²), and we therefore selected the structure with the highest resolution (3EML).

In the following, the numbering of the amino acids adheres to the arbitrary scheme of Ballesteros and Weinstein: each amino acid identifier starts with the helix number, followed by the position relative to a reference residue among the most conserved amino acids in that helix, to which the number 50 is arbitrarily assigned.⁸⁸

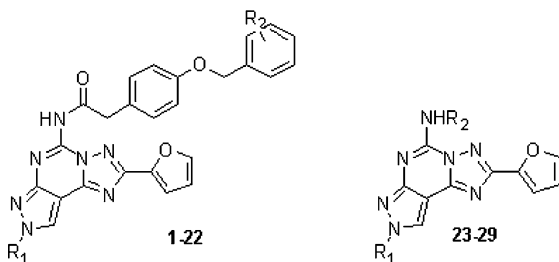
Molecular Docking of hA_{2A} AR Antagonists. Ligand structures were built using the MOE-builder tool and were subjected to MMFF94x energy minimization until the rms conjugate gradient was $<0.05 \text{ kcal mol}^{-1} \text{ \AA}^{-1}$.

In a previous study,⁸⁹ we assessed and compared the performances of the following four docking programs: MOE-Dock,⁸⁴ GOLD,⁸³ Glide,⁹⁰ and PLANTS.⁹¹ From the analysis it was shown that the docking simulations performed with GOLD give the best results in terms of lowest rmsd values between predicted and crystallographic poses of ZM 241385. On the basis of these outcomes, all of the compounds were docked into the TM binding site of the hA_{2A} AR crystal structure by using the docking tool of the GOLD suite.⁸³ For each compound, 20 independent docking runs were performed, and searching was conducted within a user-specified docking sphere with the Genetic Algorithm protocol and the GoldScore scoring function. The same docking protocol has also been recently applied to explain the binding and selectivity data at the hA₃ AR of chromone,⁹² fluorescent antagonists,⁹³ and 2-phenylphthalazin-1(2H)-ones⁹³ as well as to shed light on the effect of different substituents at the PTP scaffold on the affinity and selectivity to the hA₃ AR.⁹⁵

For each ligand, the best obtained docking pose as evaluated by the scoring function was selected to form a first data set (hereby denoted as *best* pose database). Besides, after visual inspection, for each ligand, the pose that best fits the crystallographic binding mode of ZM 241385 was selected to form a second data set (hereby denoted as *selected* pose database). Both data sets were then considered in the subsequent QSAR studies.

Interaction Energy Fingerprints. To analyze the ligand–receptor recognition mechanism in a more quantitative fashion, we calculated the individual electrostatic and hydrophobic contributions to the interaction energy of each receptor residue involved in the binding with the poses collected in the two data sets. In particular, the electrostatic contribution has been computed on the basis of the nonbonded electrostatic interaction energy term of the force field, whereas the hydrophobic contributions have been calculated by using the directional

Table 1. External Test Set



mol	R ₁	R ₂	K _i hA _{2A} (nM)
1	CH ₃	2,4-CH ₃	481 (364–635)
2	CH ₃	2,5-CH ₃	609 (456–812)
3	CH ₃	3,4-CH ₃	397 (344–458)
4	CH ₃	3,5-CH ₃	357 (273–467)
5	CH ₂ CH ₂ CH (CH ₃) ₂	2-CH ₃	52.3 (32.2–85.1)
6	CH ₂ CH ₂ CH (CH ₃) ₂	3-CH ₃	29.9 (15.3–58.1)
7	CH ₂ CH ₂ CH (CH ₃) ₂	4-CH ₃	47.3 (28.9–77.5)
8	CH ₂ CH ₂ CH (CH ₃) ₂	2,4-CH ₃	69 (44.7–107)
9	CH ₂ CH ₂ CH (CH ₃) ₂	2,5-CH ₃	75.3 (57.2–99.1)
10	CH ₂ CH ₂ CH (CH ₃) ₂	3,4-CH ₃	37.2 (35.3–39.3)
11	CH ₂ CH ₂ CH (CH ₃) ₂	3,5-CH ₃	954 (856–1060)
12	CH ₂ CH ₂ CH (CH ₃) ₂	2,4,6-CH ₃	83.7 (75.2–93.1)
13	CH ₂ CH ₂ Ph	3-CH ₃	112 (81.9–153)
14	CH ₂ CH ₂ Ph	4-CH ₃	162 (110–240)
15	CH ₂ CH ₂ Ph	2,4-CH ₃	155 (93.7–255)
16	CH ₂ CH ₂ Ph	2,5-CH ₃	52.9 (36–77.7)
17	CH ₂ CH ₂ Ph	3,4-CH ₃	109 (87.2–135)
18	CH ₂ CH ₂ Ph	3,5-CH ₃	156 (108–225)
19	CH ₂ CH ₂ CH ₂ Ph	2-CH ₃	432 (306–610)
20	CH ₂ CH ₂ CH ₂ Ph	4-CH ₃	222 (129–383)
21	CH ₂ CH ₂ CH ₂ Ph	3,4-CH ₃	8.41 (4.08–17.3)
22	CH ₃	3-CH ₃	730 (567–940)
23	CH ₃	CH ₂ CH ₂ CH ₂ O- (CH ₂ CH ₂ O) ₂ CH ₂ CH ₂ CH ₂ NH ₂	348 (269–450)
24	CH ₃	CH (CH ₃) (CH ₂) ₅ CH ₃	701 (427–1150)
25	CH ₃	CH (CH ₃)Ph (R)	38.2 (29.8–48.9)
26	CH ₃	CH ₂ Ph-3,4- (OCH ₃) ₂	64.1 (49.5–82.9)
27	CH ₃	CH ₂ CH ₂ Ph	46.1 (28.5–74.6)
28	CH ₃	CH ₂ CH ₂ -3-Indolyl	77 (42.9–138)
29	CH ₃	(CH ₂) ₅ NH ₂	52.6 (45.1–61.4)

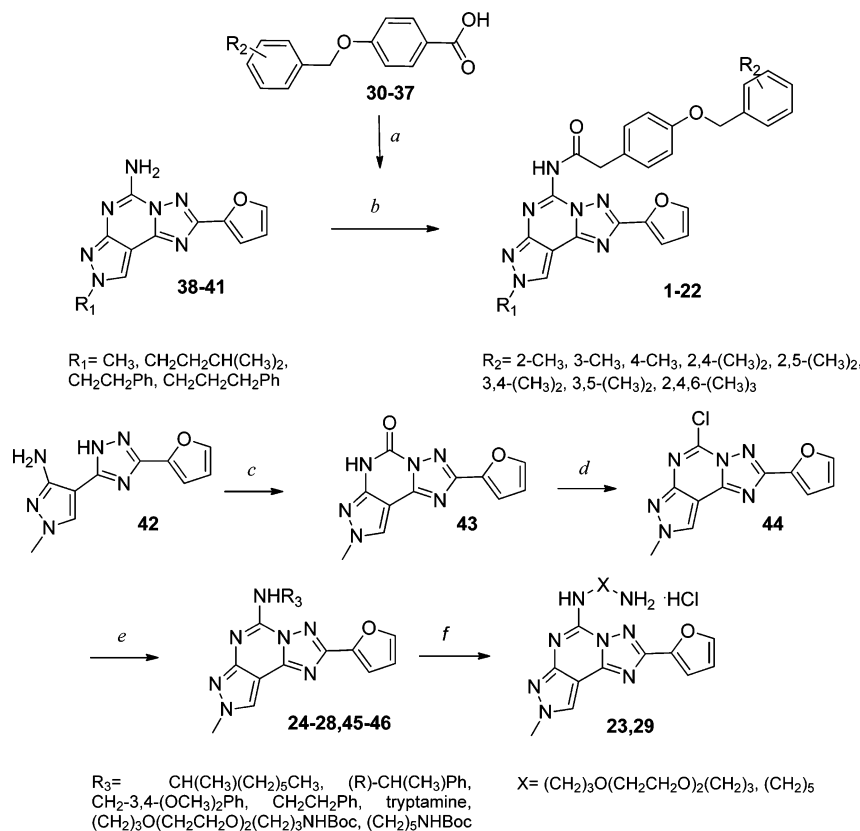
hydrophobic interaction term based on contact surfaces as implemented in the MOE scoring function. As a consequence, an energy (expressed in kcal/mol) is associated with the electrostatic contribution, whereas a score (the higher the better) is related to the hydrophobic contribution. The analysis of these contributions afforded “Interaction Energy Fingerprints” (hereby indicated as IEFs), e.g. interaction energy patterns—graphically displayed either as histograms or as 3D color maps—reporting the key residues involved in the binding with the considered ligands along with a quantitative estimate of the occurring interactions. Such analysis provides several pieces of important information at a glance. On one hand, the identification of the key residues involved in the interactions highlights possible trends in the binding modes of the considered derivatives. On the other hand, the semiquantitative analysis of the interactions allows a direct comparison of different ligands with respect to the quality of ligand–receptor contacts. The IEFs have been computed for the *selected* docking poses of the highest affinity compound for each different chemical scaffold: to estimate the electrostatic contributions, atomic charges for the ligands were calculated with MOPAC and the PM3/ESP

methodology, whereas partial charges for protein amino acids were computed with the AMBER99 force field.

Pharmacophore Model Generation. Starting with the conformations generated by the docking simulations, pharmacophore sites for each molecule were created with PHASE⁸⁵ by using the default set of chemical features, defined as follows: hydrogen bond acceptor (A), hydrogen bond donor (D), hydrophobic (H), negative ionizable (N), positive ionizable (P), and aromatic ring (R).

Once each molecule in the database was characterized with the above-described features, four-point pharmacophore hypotheses were searched through the tree-based partitioning algorithm, as implemented in PHASE.⁸⁵ In such a step, the standard procedure suggests a consideration of only a subset of the active compounds: We therefore initially attempted to consider only the most active molecule for each scaffold. This procedure, however, does not take into account any explicit knowledge about the binding to the receptor. Moreover, this choice did not lead to a common hypothesis unless it was after some of the scaffolds were removed. Consequently, to derive a common pharmacophore hypothesis consistent with all scaffolds, we

Scheme 1. Synthetic Scheme for Compounds 1–29



decided to use the crystal structure of ZM 241385 and its docked conformation as an active subset, as at least two compounds are needed to search for a common hypothesis.

The so-obtained hypotheses were filtered and scored to produce a final ranking of surviving ones. To the remaining hypotheses a survival score, which comprises different parameters such as the *alignment score*, the *vector score*, the *volume score*, and the *selectivity*, was assigned.⁸⁵ Moreover, to penalize the hypotheses not able to discriminate active compounds from inactive ones, the surviving pharmacophore hypotheses were rescored with respect to the inactive molecules.

3D-QSAR Models Generation. After a consistent pharmacophore hypothesis was defined, both *pharmacophore-based* and *atom-based* 3D-QSAR models, as available in PHASE,⁸⁵ were derived. To build the models, the ligands are first aligned to the selected pharmacophore hypothesis. Then, the space occupied by the aligned ligands is defined by a rectangular grid dividing the space into cubes of uniform size (0.5 Å each side in our specific case), and two types of 3D molecular descriptors are computed on each grid point. In the *atom-based* model, the ligands are represented by a set of overlapping van der Waals spheres (one for each atom in the ligand) classified as D, H, N, P, and W (where W refers to electron-withdrawing), whereas in the *pharmacophore-based* model the ligands are represented by spheres of specified radius, to which a category reflecting their pharmacophore features is assigned.

Therefore, the input descriptors of the QSAR analysis are represented by bits describing the cube occupancy by the pharmacophore sites and the atom types, in the *pharmacophore-based* and *atom-based* QSAR models, respectively. In *atom-based* models, the bits encode for molecular size, shape, and the above-described chemical features that have some correspondence with

pharmacophore feature types. In *pharmacophore-based* models, the bits determine which subset of pharmacophore features a molecule contains and the positions of those features with respect to the other molecules.

Partial Least Squares (PLS) analysis is then used to correlate the so-computed descriptors with the activities. As PHASE does not support the internal cross validation procedure, the original database was randomly split into selected percentages of training set and test set. Various runs with different percentages have been computed, and we finally selected 80% of compounds as the training set and 20% as the test set.

Chemistry. The compounds used as the external validation set (1–22) have been prepared by acylation with the appropriate arylacetyl chloride of the well-known and previously reported unsubstituted derivatives (38–41) in the presence of TEA in dry THF at reflux.^{43,65} Arylacetyl chlorides were obtained by treating the corresponding arylacetic acids (30–37) with an excess of oxalyl chloride and a catalytic amount of DMF in dry THF.^{96,97} Instead, derivatives 23–29 were obtained from the well-known aminotriazole (42), which was first converted to the 6-hydro-pyrazolo-triazolo-pyrimidine-5-one (43) by using diphosgene and then in the 5-chloro-derivative (44) by refluxing in POCl_3 with PCl_5 and pyridine.^{43,65,98} Final products 24–28 and the mono-Boc protected derivatives (45, 46) were prepared adding the appropriate amine to the 5-chloro-derivative in ethanol. Finally, the diamino compounds 23 and 29 were obtained by deprotection in acid of the corresponding Boc-derivatives (45, 46). In Scheme 1, the general synthetic pathway for compounds 1–29 is reported.

General. Reactions were routinely monitored by thin-layer chromatography (TLC) on silica gel (precoated F_{254} Merck plates). Flash chromatography was performed using Merck 60–200 mesh silica gel. Infrared spectra (IR) were measured on a

Jasco FT-IT instrument. ^1H NMR was determined in CDCl_3 , d_6 -DMSO, or D_2O solution with a Varian Gemini 200 spectrometer. Peaks positions are given in parts per million (δ) downfield from tetramethylsilane as an internal standard, and J values are given in Hz. The following abbreviations are used: s, singlet; bs, broad singlet; d, doublet; dd, double doublet; t, triplet; m, multiplet. Light petroleum ether refers to the fractions boiling at 40–60 °C. Melting points were determined on a Buchi-Tottoli instrument and are uncorrected.

General Procedures for the Preparation of 5-[[4(Aryloxy)]-phenyl-acetyl]amino-8-substituted-2-(2-furyl)-pyrazolo[4,3-*e*]-1,2,4-triazolo[1,5-*c*]pyrimidines (1–22). A total of 1.5 mmol of the appropriate acids (30–37) was dissolved in about 10 mL of dry THF, and then 1–2 mL of oxalylchloride and 0.1 mL of DMF were added. The resulting mixture was stirred at room temperature for 2–3 h. After that, the solvent was removed under reduced pressure, obtaining the corresponding acyl chlorides. Then, to a solution of acylchloride in dry THF were added 0.3 mmol of the appropriate 5-amino-pyrazolo-triazolo-pyrimidine (38–41) and 1.5 mmol of TEA. The reaction was refluxed overnight. The solvent was removed under reduced pressure, and to the residue was added ethyl acetate, which was washed three times with NaHCO_3 aq. The organic layer was dried, concentrated, and purified by flash chromatography.

5-[[4(3-Methylbenzyloxy)]phenyl-acetyl]amino-8-methyl-2-(2-furyl)-pyrazolo[4,3-*e*]1,2,4-triazolo[1,5-*c*]pyrimidine (1). Yield 67%; yellow solid. mp 180 °C (EtOAc-light petroleum). IR (KBr): 3250–2990, 1684, 1617, 1565, 1500 cm^{-1} . ^1H NMR (CDCl_3) δ : 2.37 (s, 3H), 4.22 (s, 3H), 4.46 (s, 2H), 5.02 (s, 2H), 6.61 (dd, 1H, $J = 2$, $J = 4$), 7.00 (d, 2H, $J = 7$), 7.16 (d, 1H, $J = 4$), 7.26–7.41 (m, 6H), 7.64 (d, 1H, $J = 2$), 8.21 (s, 1H), 9.09 (s, 1H).

5-[[4(2,4-Dimethylbenzyloxy)]phenyl-acetyl]amino-8-methyl-2-(2-furyl)-pyrazolo[4,3-*e*]1,2,4-triazolo[1,5-*c*]pyrimidine (2). Yield 63%; yellow solid. mp 170 °C (EtOAc-light petroleum). IR (KBr): 3248–2986, 1682, 1610, 1563, 1500 cm^{-1} . ^1H NMR (CDCl_3) δ : 2.17 (s, 3H), 2.32 (s, 3H), 4.21 (s, 3H), 4.46 (s, 2H), 4.98 (s, 2H), 6.59 (dd, 1H, $J = 2$, $J = 4$), 6.97–7.04 (m, 4H), 7.19–7.36 (m, 4H), 7.64 (d, 1H, $J = 2$), 8.21 (s, 1H), 9.09 (s, 1H).

5-[[4(2,5-Dimethylbenzyloxy)]phenyl-acetyl]amino-8-methyl-2-(2-furyl)-pyrazolo[4,3-*e*]1,2,4-triazolo[1,5-*c*]pyrimidine (3). Yield 71%; yellow solid. mp 180 °C (EtOAc-light petroleum). IR (KBr): 3253–2990, 1678, 1615, 1560, 1510 cm^{-1} . ^1H NMR (CDCl_3) δ : 2.31 (s, 6H), 4.21 (s, 3H), 4.47 (s, 2H), 4.98 (s, 2H), 6.60 (dd, 1H, $J = 2$, $J = 4$), 6.98–7.09 (m, 4H), 7.21–7.36 (m, 4H), 7.64 (d, 1H, $J = 2$), 8.21 (s, 1H), 9.10 (s, 1H).

5-[[4(3,4-Dimethylbenzyloxy)]phenyl-acetyl]amino-8-methyl-2-(2-furyl)-pyrazolo[4,3-*e*]1,2,4-triazolo[1,5-*c*]pyrimidine (4). Yield 65%; yellow solid. mp 185 °C (EtOAc-light petroleum). IR (KBr): 3245–2985, 1680, 1612, 1568, 1505 cm^{-1} . ^1H NMR (CDCl_3) δ : 2.27 (s, 6H), 4.21 (s, 3H), 4.47 (s, 2H), 4.98 (s, 2H), 6.60 (dd, 1H, $J = 2$, $J = 4$), 7.00 (bs, 3H), 7.15–7.28 (m, 5H), 7.64 (d, 1H, $J = 2$), 8.21 (s, 1H), 9.09 (s, 1H).

5-[[4(3,5-Dimethylbenzyloxy)]phenyl-acetyl]amino-8-methyl-2-(2-furyl)-pyrazolo[4,3-*e*]1,2,4-triazolo[1,5-*c*]pyrimidine (5). Yield 66%; yellow solid. mp 165 °C (EtOAc-light petroleum). IR (KBr): 3250–2993, 1677, 1610, 1562, 1500 cm^{-1} . ^1H NMR (CDCl_3) δ : 2.32 (s, 6H), 4.21 (s, 3H), 4.46 (s, 2H), 4.97 (s, 2H), 6.60 (dd, 1H, $J = 2$, $J = 4$), 6.97–7.04 (m, 4H), 7.25–7.40 (m, 4H), 7.64 (d, 1H, $J = 2$), 8.21 (s, 1H), 9.10 (s, 1H).

5-[[4(2-Methylbenzyloxy)]phenyl-acetyl]amino-8-isopentyl-2-(2-furyl)-pyrazolo[4,3-*e*]1,2,4-triazolo[1,5-*c*]pyrimidine (6). Yield 77%; yellow solid. mp 80 °C (EtOAc-light petroleum).

IR (KBr): 3252–2990, 1682, 1608, 1563, 1504 cm^{-1} . ^1H NMR (CDCl_3) δ : 0.98 (d, 6H, $J = 6.6$), 1.57 (m, 1H), 1.91 (q, 2H, $J = 7$), 2.36 (s, 3H), 4.37–4.47 (m, 4H), 5.02 (s, 2H), 6.60 (dd, 1H, $J = 2$, $J = 4$), 7.01–7.03 (m, 2H), 7.23–7.39 (m, 7H), 7.62 (d, 1H, $J = 2$), 8.22 (s, 1H), 9.11 (s, 1H).

5-[[4(3-Methylbenzyloxy)]phenyl-acetyl]amino-8-isopentyl-2-(2-furyl)-pyrazolo[4,3-*e*]1,2,4-triazolo[1,5-*c*]pyrimidine (7). Yield 62%; yellow solid. mp 70 °C (EtOAc-light petroleum). IR (KBr): 3247–2990, 1681, 1610, 1565, 1500 cm^{-1} . ^1H NMR (CDCl_3) δ : 0.98 (d, 6H, $J = 6.6$), 1.57 (m, 1H), 1.91 (q, 2H, $J = 7$), 2.36 (s, 3H), 4.37–4.45 (m, 4H), 5.01 (s, 2H), 6.59 (dd, 1H, $J = 2$, $J = 4$), 6.96–7.00 (m, 2H), 7.15–7.34 (m, 7H), 7.62 (d, 1H, $J = 2$), 8.22 (s, 1H), 9.09 (s, 1H).

5-[[4(4-Methylbenzyloxy)]phenyl-acetyl]amino-8-isopentyl-2-(2-furyl)-pyrazolo[4,3-*e*]1,2,4-triazolo[1,5-*c*]pyrimidine (8). Yield 69%; white solid. mp 80 °C (EtOAc-light petroleum). IR (KBr): 3250–2990, 1681, 1612, 1570, 1508 cm^{-1} . ^1H NMR (CDCl_3) δ : 0.98 (d, 6H, $J = 6.6$), 1.60 (m, 1H), 1.93 (q, 2H, $J = 7$), 2.36 (s, 3H), 4.37–4.45 (m, 4H), 5.01 (s, 2H), 6.59 (dd, 1H, $J = 2$, $J = 4$), 6.96 (d, 4H, $J = 8.8$), 7.16–7.33 (m, 5H), 7.64 (d, 1H, $J = 2$), 8.22 (s, 1H), 9.10 (s, 1H).

5-[[4(2,4-Dimethylbenzyloxy)]phenyl-acetyl]amino-8-isopentyl-2-(2-furyl)-pyrazolo[4,3-*e*]1,2,4-triazolo[1,5-*c*]pyrimidine (9). Yield 62%; pale yellow solid. mp 85 °C (EtOAc-light petroleum). IR (KBr): 3255–2995, 1680, 1615, 1572, 1510 cm^{-1} . ^1H NMR (CDCl_3) δ : 0.98 (d, 6H, $J = 6.6$), 1.58 (m, 1H), 1.91 (m, 2H), 2.33 (s, 6H), 4.41–4.46 (m, 4H), 4.98 (s, 2H), 6.59 (dd, 1H, $J = 2$, $J = 4$), 7.01–7.04 (m, 5H), 7.23–7.40 (m, 3H), 7.64 (d, 1H, $J = 2$), 8.22 (s, 1H), 9.10 (s, 1H).

5-[[4(2,5-Dimethylbenzyloxy)]phenyl-acetyl]amino-8-isopentyl-2-(2-furyl)-pyrazolo[4,3-*e*]1,2,4-triazolo[1,5-*c*]pyrimidine (10). Yield 68%; yellow solid. mp 75 °C (EtOAc-light petroleum). IR (KBr): 3248–2986, 1675, 1610, 1571, 1512 cm^{-1} . ^1H NMR (CDCl_3) δ : 0.98 (d, 6H, $J = 6.6$), 1.62 (m, 1H), 1.93 (q, 2H, $J = 7$), 2.32 (s, 6H), 4.37–4.47 (m, 4H), 4.98 (s, 2H), 6.59 (dd, 1H, $J = 2$, $J = 4$), 6.98–7.09 (m, 4H), 7.20–7.36 (m, 4H), 7.64 (d, 1H, $J = 2$), 8.23 (s, 1H), 9.09 (s, 1H).

5-[[4(3,4-Dimethylbenzyloxy)]phenyl-acetyl]amino-8-isopentyl-2-(2-furyl)-pyrazolo[4,3-*e*]1,2,4-triazolo[1,5-*c*]pyrimidine (11). Yield 77%; white solid. mp 78 °C (EtOAc-light petroleum). IR (KBr): 3249–2993, 1679, 1614, 1570, 1500 cm^{-1} . ^1H NMR (CDCl_3) δ : 0.98 (d, 6H, $J = 6.6$), 1.60 (m, 1H), 1.93 (q, 2H, $J = 7$), 2.26 (s, 6H), 4.37–4.47 (m, 4H), 4.98 (s, 2H), 6.60 (dd, 1H, $J = 2$, $J = 4$), 6.96–7.02 (m, 3H), 7.15–7.33 (m, 5H), 7.64 (d, 1H, $J = 2$), 8.22 (s, 1H), 9.11 (s, 1H).

5-[[4(3,5-Dimethylbenzyloxy)]phenyl-acetyl]amino-8-isopentyl-2-(2-furyl)-pyrazolo[4,3-*e*]1,2,4-triazolo[1,5-*c*]pyrimidine (12). Yield 82%; white solid. mp 55 °C (EtOAc-light petroleum). IR (KBr): 3250–2990, 1680, 1615, 1567, 1513 cm^{-1} . ^1H NMR (CDCl_3) δ : 0.98 (d, 6H, $J = 6.6$), 1.62 (m, 1H), 1.93 (q, 2H, $J = 7$), 2.32 (s, 6H), 4.37–4.45 (m, 4H), 4.97 (s, 2H), 6.59 (dd, 1H, $J = 2$, $J = 4$), 6.96–7.04 (m, 4H), 7.19 (d, 1H, $J = 4$), 7.26–7.34 (m, 3H), 7.64 (d, 1H, $J = 2$), 8.22 (s, 1H), 9.10 (s, 1H).

5-[[4(2,4,6-Trimethylbenzyloxy)]phenyl-acetyl]amino-8-isopentyl-2-(2-furyl)-pyrazolo[4,3-*e*]1,2,4-triazolo[1,5-*c*]pyrimidine (13). Yield 56%; yellow solid. mp 70 °C (EtOAc-light petroleum). IR (KBr): 3260–2995, 1674, 1608, 1563, 1501 cm^{-1} . ^1H NMR (CDCl_3) δ : 0.98 (d, 6H, $J = 6.6$), 1.60 (m, 1H), 1.93 (q, 2H, $J = 7$), 2.28 (s, 3H), 2.35 (s, 6H), 4.37–4.48 (m, 4H), 4.99 (s, 2H), 6.60 (dd, 1H, $J = 2$, $J = 4$), 6.90 (s, 2H), 7.01 (d, 2H, $J = 8.6$), 7.23–7.36 (m, 3H), 7.64 (d, 1H, $J = 2$), 8.23 (s, 1H), 9.11 (s, 1H).

5-[[4(3-Methylbenzyloxy)]phenyl-acetyl]amino-8-(2-phenylethyl)-2-(2-furyl)-pyrazolo[4,3-*e*]1,2,4-triazolo[1,5-*c*]pyrimidine (**14**). Yield 71%; yellow solid. mp 70 °C (EtOAc-light petroleum). IR (KBr): 3255–2995, 1676, 1610, 1560, 1513 cm⁻¹. ¹H NMR (CDCl₃) δ: 2.37 (s, 3H), 3.32 (t, 2H, *J* = 6), 4.46 (s, 2H), 4.60 (t, 2H, *J* = 6), 5.02 (s, 2H), 6.58 (dd, 1H, *J* = 2, *J* = 4), 7.02–7.08 (m, 4H), 7.16–7.35 (m, 10H), 7.62 (d, 1H, *J* = 2), 7.88 (s, 1H), 9.10 (s, 1H).

5-[[4(4-Methylbenzyloxy)]phenyl-acetyl]amino-8-(2-phenylethyl)-2-(2-furyl)-pyrazolo[4,3-*e*]1,2,4-triazolo[1,5-*c*]pyrimidine (**15**). Yield 75%; white solid. mp 70 °C (EtOAc-light petroleum). IR (KBr): 3247–2980, 1675, 1612, 1562, 1500 cm⁻¹. ¹H NMR (CDCl₃) δ: 2.35 (s, 3H), 3.32 (t, 2H, *J* = 6.6), 4.45 (s, 2H), 4.60 (t, 2H, *J* = 6.6), 5.01 (s, 2H), 6.59 (dd, 1H, *J* = 2, *J* = 4), 6.97–7.08 (m, 3H), 7.17–7.35 (m, 11H), 7.62 (d, 1H, *J* = 2), 7.88 (s, 1H), 9.10 (s, 1H).

5-[[4(2,4-Dimethylbenzyloxy)]phenyl-acetyl]amino-8-(2-phenylethyl)-2-(2-furyl)-pyrazolo[4,3-*e*]1,2,4-triazolo[1,5-*c*]pyrimidine (**16**). Yield 66%; yellow solid. mp 90 °C (EtOAc-light petroleum). IR (KBr): 3250–2994, 1682, 1610, 1571, 1510 cm⁻¹. ¹H NMR (CDCl₃) δ: 2.32 (s, 6H), 3.32 (t, 2H, *J* = 7), 4.46 (s, 2H), 4.60 (t, 2H, *J* = 7), 4.99 (s, 2H), 6.58 (dd, 1H, *J* = 2, *J* = 4), 6.98–7.04 (m, 5H), 7.17 (d, 1H, *J* = 4), 7.27–7.36 (m, 7H), 7.62 (d, 1H, *J* = 2), 7.88 (s, 1H), 9.11 (s, 1H).

5-[[4(2,5-Dimethylbenzyloxy)]phenyl-acetyl]amino-8-(2-phenylethyl)-2-(2-furyl)-pyrazolo[4,3-*e*]1,2,4-triazolo[1,5-*c*]pyrimidine (**17**). Yield 73%; white solid. mp 90 °C (EtOAc-light petroleum). IR (KBr): 3251–2990, 1677, 1609, 1570, 1505 cm⁻¹. ¹H NMR (CDCl₃) δ: 2.32 (s, 6H), 3.33 (t, 2H, *J* = 7), 4.47 (s, 2H), 4.61 (t, 2H, *J* = 7), 4.98 (s, 2H), 6.60 (dd, 1H, *J* = 2, *J* = 4), 7.00–7.37 (m, 13H), 7.63 (d, 1H, *J* = 2), 7.88 (s, 1H), 9.10 (s, 1H).

5-[[4(3,4-Dimethylbenzyloxy)]phenyl-acetyl]amino-8-(2-phenylethyl)-2-(2-furyl)-pyrazolo[4,3-*e*]1,2,4-triazolo[1,5-*c*]pyrimidine (**18**). Yield 73%; pale yellow solid. mp 65 °C (EtOAc-light petroleum). IR (KBr): 3248–2989, 1680, 1612, 1575, 1508 cm⁻¹. ¹H NMR (CDCl₃) δ: 2.27–2.32 (m, 6H), 3.33 (t, 2H, *J* = 6.2), 4.45 (s, 2H), 4.61 (t, 2H, *J* = 6.2), 4.98 (s, 2H), 6.58 (dd, 1H, *J* = 2, *J* = 4), 6.97–7.07 (m, 4H), 7.15–7.35 (m, 9H), 7.63 (d, 1H, *J* = 2), 7.89 (s, 1H), 9.09 (s, 1H).

5-[[4(3,5-Dimethylbenzyloxy)]phenyl-acetyl]amino-8-(2-phenylethyl)-2-(2-furyl)-pyrazolo[4,3-*e*]1,2,4-triazolo[1,5-*c*]pyrimidine (**19**). Yield 80%; white solid. mp 75 °C (EtOAc-light petroleum). IR (KBr): 3253–2980, 1675, 1614, 1573, 1500 cm⁻¹. ¹H NMR (CDCl₃) δ: 2.32 (s, 6H), 3.33 (t, 2H, *J* = 7), 4.46 (s, 2H), 4.60 (t, 2H, *J* = 7), 4.98 (s, 2H), 6.58 (dd, 1H, *J* = 2, *J* = 4), 6.97–7.04 (m, 5H), 7.16 (d, 1H, *J* = 4), 7.26–7.35 (m, 7H), 7.62 (d, 1H, *J* = 2), 7.88 (s, 1H), 9.10 (s, 1H).

5-[[4(2-Methylbenzyloxy)]phenyl-acetyl]amino-8-(3-phenylpropyl)-2-(2-furyl)-pyrazolo[4,3-*e*]1,2,4-triazolo[1,5-*c*]pyrimidine (**20**). Yield 75%; pale yellow solid. mp 80 °C (EtOAc-light petroleum). IR (KBr): 3250–2990, 1677, 1615, 1573, 1512 cm⁻¹. ¹H NMR (CDCl₃) δ: 2.36–2.46 (m, 5H), 2.66 (t, 2H, *J* = 7), 4.37 (t, 2H, *J* = 7), 4.46 (s, 2H), 5.02 (s, 2H), 6.60 (dd, 1H, *J* = 2, *J* = 4), 7.00 (d, 2H, *J* = 8.4), 7.21–7.36 (m, 12H), 7.64 (d, 1H, *J* = 2), 8.19 (s, 1H), 9.11 (s, 1H).

5-[[4(4-Methylbenzyloxy)]phenyl-acetyl]amino-8-(3-phenylpropyl)-2-(2-furyl)-pyrazolo[4,3-*e*]1,2,4-triazolo[1,5-*c*]pyrimidine (**21**). Yield 75%; yellow solid. mp 70 °C (EtOAc-light petroleum). IR (KBr): 3250–2978, 1672, 1610, 1580, 1510 cm⁻¹. ¹H NMR (CDCl₃) δ: 2.35–2.42 (m, 5H), 2.66 (t, 2H, *J* = 7), 4.37 (t, 2H, *J* = 7), 4.44 (s, 2H), 5.01 (s, 2H), 6.60 (dd, 1H, *J* = 2, *J* = 4),

6.98 (d, 2H, *J* = 8), 7.20–7.34 (m, 12H), 7.64 (d, 1H, *J* = 2), 8.18 (s, 1H), 9.10 (s, 1H).

5-[[4(3,4-Dimethylbenzyloxy)]phenyl-acetyl]amino-8-(3-phenylpropyl)-2-(2-furyl)-pyrazolo[4,3-*e*]1,2,4-triazolo[1,5-*c*]pyrimidine (**22**). Yield 67%; brown solid. mp 67 °C (EtOAc-light petroleum). IR (KBr): 3245–2987, 1681, 1615, 1568, 1513 cm⁻¹. ¹H NMR (CDCl₃) δ: 2.26–2.31 (m, 6H), 2.39 (m, 2H), 2.66 (t, 2H, *J* = 7), 4.34–4.43 (m, 4H), 4.98 (s, 2H), 6.59 (dd, 1H, *J* = 2, *J* = 4), 6.98 (d, 2H, *J* = 8.2), 7.14–7.34 (m, 11H), 7.64 (d, 1H, *J* = 2), 8.20 (s, 1H), 9.10 (s, 1H).

Synthesis of the 2-Furan-2-yl-8-methyl-6-hydro-pyrazolo[4,3-*e*][1,2,4]triazolo[1,5-*c*]pyrimidin-5-one (43**).** Compound **42** (200 mg, 0.869 mmol) was dissolved in dry dioxane, and diphosgene was added (1.13 mmol, 0.136 mL). The mixture was heated at 70 °C for 1.5 h. The reaction was monitored by TLC (EtOAc-MeOH 9:1), and when the starting material disappeared the solvent was removed. The product (**43**) was precipitated (EtOAc-light petroleum), obtaining an ivory powder that was used without further purification. Yield 46%; ivory solid. mp >300 °C (EtOAc-light petroleum). IR (KBr): 1700, 1613, 1582, 1510 cm⁻¹. ¹H NMR (d₆-DMSO) δ: 3.96 (3H, s), 6.71 (1H, dd, *J* = 2, *J* = 4), 7.18 (1H, d, *J* = 4), 7.93 (1H, d, *J* = 2), 8.58 (1H, s). ES-MS (methanol): 279.00 (M+23).

Synthesis of the 5-Chloro-2-furan-2-yl-8-methyl-pyrazolo[4,3-*e*][1,2,4]triazolo[1,5-*c*]pyrimidine (44**).** Compound **43** (100 mg, 0.390 mmol) was dissolved in phosphoryl chloride (21.46 mmol, 2 mL), and phosphorus pentachloride (0.117 mmol, 24 mg) and pyridine (0.975 mmol, 0.079 mL) were added. The mixture was refluxed for 24 h; then the solvent was removed under reduced pressure, and the residue was dissolved in chloroform and washed with water and brine (1:1). The organic layer was dried and concentrated and purified through flash chromatography using 9.5:0.5 EtOAc–MeOH to yield the desired compound (**44**). Yield 34%; white solid. mp 285 °C (EtOAc-light petroleum). IR (KBr): 1610, 1575, 1502, 580 cm⁻¹. ¹H NMR (d₆-DMSO) δ: 4.12 (3H, s), 6.73 (1H, dd, *J* = 2, *J* = 4), 7.22 (1H, d, *J* = 4), 7.95 (1H, d, *J* = 2), 8.61 (1H, s). ES-MS (methanol): 297.00 (M+23).

General Procedure for the Synthesis of the 5-Amino-substituted-2-furan-2-yl-8-methyl-pyrazolo[4,3-*e*][1,2,4]triazolo[1,5-*c*]pyrimidine (24–28, 45–46**).** 5-Chloro-derivative **44** (100 mg, 0.364 mmol) was dissolved in 5 mL of ethanol in a tube. Triethylamine (TEA, 0.364 mmol, 51 μL) and the appropriate amine (1.092 mmol) were added to the mixture; the tube was closed and heated at 110 °C for 2 h. The reaction was monitored through TLC (EtOAc-MeOH 9:1). After the reaction was completed, the solvent was removed under pressure and the residue purified by flash chromatography (EtOAc-MeOH 9.5:0.5) yielding the desired compound.

(2-Furan-2-yl-8-methyl-pyrazolo[4,3-*e*][1,2,4]triazolo[1,5-*c*]pyrimidin-5-yl)-(1-methyl-heptyl)-amine (24**).** Yield 84%; yellow solid. mp 149 °C (EtOAc-light petroleum). IR (KBr): 3224–2988, 1610, 1579, 1505 cm⁻¹. ¹H NMR (CDCl₃) δ: 0.85 (3H, t, *J* = 7), 1.13–1.55 (11H, m), 1.57–1.73 (2H, m), 4.09 (3H, s), 4.33–4.55 (1H, m), 5.81 (1H, d, *J* = 9), 6.60 (1H, dd, *J* = 2, *J* = 4), 7.22 (1H, d, *J* = 4), 7.63 (1H, d, *J* = 2), 8.09 (1H, s).

(R)-(2-Furan-2-yl-8-methyl-pyrazolo[4,3-*e*][1,2,4]triazolo[1,5-*c*]pyrimidin-5-yl)-(1-phenyl-ethyl)-amine (25**).** Yield 92%; yellow solid. mp 69 °C (EtOAc-light petroleum). IR (KBr): 3320–3260, 1610, 1575, 1502 cm⁻¹. ¹H NMR (CDCl₃) δ: 1.72 (3H, d, *J* = 7), 4.09 (3H, s), 5.47–5.62 (1H, m), 6.48–6.63 (2H, m), 7.20–7.51 (5H, m), 7.61 (1H, d, *J* = 2), 8.06 (1H, s).

(3,4-Dimethoxy-benzyl)-(2-furan-2-yl-8-methyl-pyrazolo[4,3-e][1,2,4]triazolo[1,5-c]pyrimidin-5-yl)-amine (**26**). Yield 74%; yellow solid. mp 109 °C (EtOAc-light petroleum). IR (KBr): 3315–3265, 1615, 1582, 1510 cm⁻¹. ¹H NMR (CDCl₃) δ: 3.88 (6H, s), 4.12 (3H, s), 4.80 (2H, d, *J* = 5), 6.45–6.62 (2H, m), 6.83 (1H, d, *J* = 7), 6.93–7.05 (2H, m), 7.19 (1H, d, *J* = 4), 7.60 (1H, d, *J* = 2), 8.10 (1H, s).

(2-Furan-2-yl-8-methyl-pyrazolo[4,3-e][1,2,4]triazolo[1,5-c]pyrimidin-5-yl)-phenethyl-amine (**27**). Yield 76%; pale brown solid. mp 120 °C (EtOAc-light petroleum). IR (KBr): 3230–2990, 1608, 1583, 1514 cm⁻¹. ¹H NMR (CDCl₃) δ: 3.08 (2H, t, *J* = 7), 3.89–3.96 (2H, m), 4.11 (3H, s), 5.34 (1H, bs), 6.58 (1H, dd, *J* = 2, *J* = 4), 7.16–7.37 (6H, m), 7.59 (1H, d, *J* = 2), 8.09 (1H, s).

(2-Furan-2-yl-8-methyl-pyrazolo[4,3-e][1,2,4]triazolo[1,5-c]pyrimidin-5-yl)-[2-(1*H*-indol-3-yl)-ethyl]-amine (**28**). Yield 67%; pale brown solid. mp 160 °C (EtOAc-light petroleum). IR (KBr): 3233–2998, 1612, 1581, 1502 cm⁻¹. ¹H NMR (CDCl₃) δ: 3.25 (2H, t, *J* = 7), 4.00–4.14 (5H, m), 6.54 (1H, bs), 6.60 (1H, dd, *J* = 2, *J* = 4), 6.93–7.22 (2H, m), 7.39 (2H, d, *J* = 6), 7.50–7.68 (2H, m), 8.11 (1H, bs), 8.33 (1H, s).

[3-{2-[3-(2-Furan-2-yl-8-methyl-pyrazolo[4,3-e][1,2,4]triazolo[1,5-c]pyrimidin-5-ylamino)-propoxy]-ethoxy}-ethoxy)-propyl]-carbamic acid tert-butyl ester (**45**). Yield 67%; pale pink solid. mp 69 °C (EtOAc-light petroleum). IR (KBr): 3230–2995, 1725, 1611, 1588, 1513 cm⁻¹. ¹H NMR (CDCl₃) δ: 1.44 (9H, s), 1.68–1.82 (2H, m), 1.96–2.15 (2H, m), 3.24 (2H, bs), 3.51–3.86 (14H, m), 4.12 (3H, s), 5.00 (1H, bs), 6.60 (1H, dd, *J* = 2, *J* = 4), 6.84 (1H, bs), 7.22 (1H, d, *J* = 4), 7.62 (1H, d, *J* = 2), 8.08 (1H, s).

[5-(2-Furan-2-yl-8-methyl-pyrazolo[4,3-e][1,2,4]triazolo[1,5-c]pyrimidin-5-ylamino)-pentyl]-carbamic acid tert-butyl ester (**46**). Yield 82%; white solid. mp 119 °C (EtOAc-light petroleum). IR (KBr): 3235–2993, 1723, 1608, 1580, 1509 cm⁻¹. ¹H NMR (CDCl₃) δ: 1.43–1.82 (15H, m), 3.08–3.18 (2H, m), 3.69 (2H, dd, *J* = 7, *J* = 14), 4.11 (3H, s), 4.54 (1H, bs), 6.27 (1H, bs), 6.60 (1H, dd, *J* = 2, *J* = 4), 7.22 (1H, d, *J* = 4), 7.63 (1H, d, *J* = 2), 8.09 (1H, s). ES-MS (methanol) *m/z*: 463.2 (*M* + 23).

General Procedure for the N-Boc Deprotection (23, 29). Tertbutoxycarbonyl derivatives (100 mg) **45–46** were dissolved in EtOAc saturated by HCl_(g) (5 mL) and stirred at room temperature for 1 h. Reaction was monitored by TLC (EtOAc-MeOH 9:1). Solvent was then removed under reduced pressure and the desired compound (**23,29**) was filtered off.

3-{2-[3-(2-Furan-2-yl-8-methyl-pyrazolo[4,3-e][1,2,4]triazolo[1,5-c]pyrimidin-5-ylamino)-propoxy]-ethoxy}-ethoxy)-propyl-ammonium; chloride (**23**). Yield 56%; sticky foam. IR (KBr): 3349, 3228–2994, 1615, 1576, 1507 cm⁻¹. ¹H NMR (D₂O) δ: 1.87–1.99 (4H, m), 3.05 (2H, t, *J* = 7), 3.55–3.75 (14H, m), 3.97 (3H, s), 6.62 (1H, dd, *J* = 2, *J* = 4), 6.99 (1H, d, *J* = 4), 7.65 (1H, d, *J* = 2), 8.08 (1H, s).

5-(2-Furan-2-yl-8-methyl-pyrazolo[4,3-e][1,2,4]triazolo[1,5-c]pyrimidin-5-ylamino)-pentyl-ammonium; chloride (**29**). Yield 73%; pale yellow solid. mp 126 °C (EtOAc-light petroleum). IR (KBr): 3355, 3225–3002, 1610, 1583, 1504 cm⁻¹. ¹H NMR (D₂O) δ: 1.41–1.56 (2H, m), 1.70–1.74 (4H, m), 3.03 (2H, t, *J* = 7), 3.37 (2H, t, *J* = 7), 3.91 (3H, s), 6.56 (1H, dd, *J* = 2, *J* = 4), 6.88 (1H, d, *J* = 4), 7.58 (1H, d, *J* = 2), 7.95 (1H, s).

Biological Assays. Binding at the hA_{2A} AR was evaluated for all the newly synthesized PTP compounds (**1–29**): the affinity was determined by measuring the displacement of specific [³H]NECA binding at the hA_{2A} AR expressed in Chinese

Hamster Ovary cells (CHO) cells. Data are expressed in terms of *K_i* (dissociation constant), with geometric means of at least 3 experiments, including 95% confidence intervals.

RESULTS AND DISCUSSION

It is generally accepted that the integration of *ligand-* and *structure-based* strategies might sensitively increase the success rate of the drug candidates' identification process. In fact, *ligand-based* methods find wide and successful application in the development of quantitative models able to correlate and predict biological activities based on different molecular properties. On the other hand, molecular docking represents a robust strategy to exhaustively explore the conformational space of a ligand inside its binding cavity, inferring the possible ligand "bioactive" conformation. Within this framework, conformations generated by docking simulations might represent the natural "structural" input for 3D-QSAR strategies such as CoMFA or 3D-pharmacophore search, when no experimental "bioactive" pose is available.

Also in this case study, the driving force that pushed us to explore the performance of an integrated *ligand-* and *structure-based* 3D-QSAR approach came from our initial attempt to derive a conventional ligand-based pharmacophore hypothesis of all 751 hA_{2A} AR antagonists collected from the literature without taking into account any available crystallographic information. We therefore let PHASE⁸⁵ perform the conformational search of the structures in the database. Due to the high number of molecules in the data set, however, the number of outcoming conformers was not manageable. As a consequence, it was only possible to generate models for rather small subsets of molecules and not a general one. In this view, the proposed combined strategy represents, with all its limitations, the best computationally feasible strategy to derive models when managing with data sets of a discrete size, as the use of conformations generated by the docking algorithms allows also a reduction of the computational cost of the 3D-QSAR procedure.

Consequently, the starting point of our alternative integrated approach has been therefore the molecular docking of all 751 hA_{2A} AR antagonists collected from the literature, to obtain the input molecular conformations for the subsequent pharmacophore hypotheses and 3D-QSAR model generation. According to the best docking performance obtained in a previous study⁸⁹ and to the higher structural similarity the scaffolds in our database share with ZM 241385 when compared to the other cocrystallized antagonists, all the selected compounds have been subjected to docking simulations into the binding cavity of the A_{2A} AR crystal structure in complex with the latter²⁸ by using the GOLD software package.⁸³

From the conformations generated by the docking algorithm, two data sets were derived, each containing one docking pose per compound: the *best* pose and the *selected* pose databases. For the first data set, the best poses in terms of GoldScore fitness were selected, whereas for the second database for each compound the pose that best reproduces important interactions observed for the crystallographic binding mode of ZM 241385 was selected. In particular, the key interactions that have been identified are two hydrogen bonds with Asn253 (6.55), an aromatic π - π stacking interaction with Phe168 (EL2), and a hydrogen bond with the Glu169 (EL2) side chains. Interestingly, with regard to these interactions, the *best* and *selected* poses frequently overlapped (546/751 molecules).

Moreover, to analyze the ligand-receptor recognition mechanism in a more quantitative fashion, we calculated the individual electrostatic and hydrophobic contributions to the interaction energy of each receptor residue involved in the

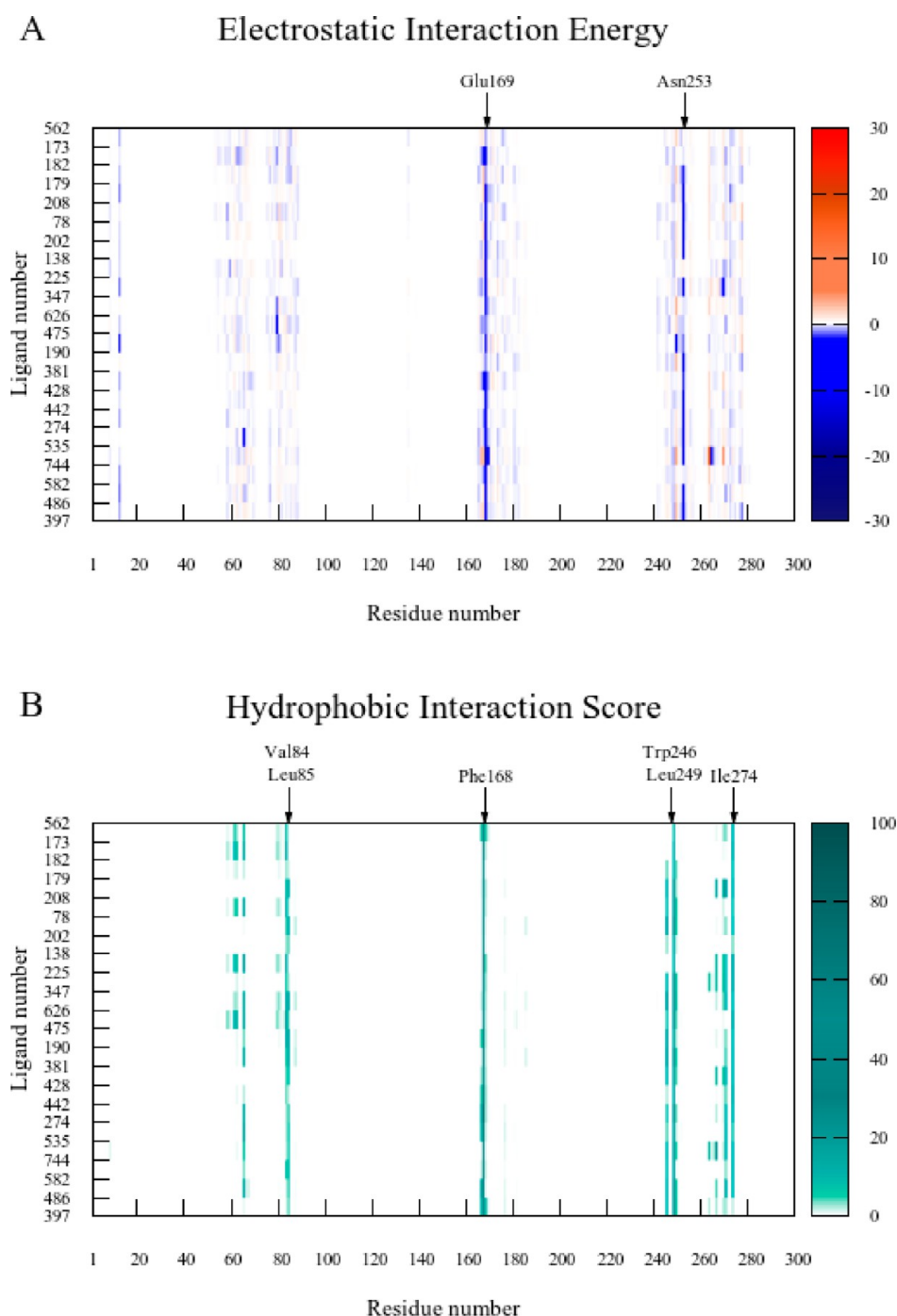


Figure 3. (A) *Per residue* electrostatic interaction energy fingerprint and (B) *per residue* hydrophobic interaction score fingerprint. The maps are calculated considering the selected poses, obtained after docking at the hA_{2A} AR, of the highest affinity compounds for each different scaffold. Electrostatic energy values are expressed in kcal/mol, while hydrophobic scores are expressed in arbitrary hydrophobic units. The selected molecules per scaffold are mol397 (scaffold O), mol486 (scaffold F), mol582 (scaffold A), mol744 (scaffold Q), mol535 (scaffold G), mol274 (scaffold L), mol442 (scaffold V), mol428 (scaffold R), mol381 (scaffold N), mol190 (scaffold D), mol475 (scaffold K), mol626 (scaffold P), mol347 (scaffold B), mol225 (scaffold J), mol138 (scaffold U), mol202 (scaffold M), mol78 (scaffold C), mol208 (scaffold S), mol179 (scaffold I), mol182 (scaffold T), mol173 (scaffold E), mol562 (scaffold H). Molecules are ordered in the map by their K_i values at the hA_{2A} AR, from the lowest (bottom) to the highest (top).

binding with the ligands. For this purpose, the analysis has been narrowed to the *selected* poses of the compounds showing the highest affinity for each different chemical scaffold. With the calculated *per residue* electrostatic and hydrophobic energy interaction contributions values, the color maps depicted in Figure 3 were derived.

The *per residue* electrostatic IEF (Figure 3A) shows two main bands with negative energy (colored in blue) corresponding to

Glu169 (EL2) and Asn253 (6.55), indicating that these residues are responsible for the main electrostatic interactions with the selected compounds. Only a few compounds are not predicted to strongly interact with both of these residues, namely mol744, mol626, mol347, mol138, and mol173. However, although they do not interact with Asn253 (6.55), they still establish favorable interactions with Glu169 (EL2). On the other hand, the map of the *per residue* hydrophobic IEF (Figure 3B) highlights several

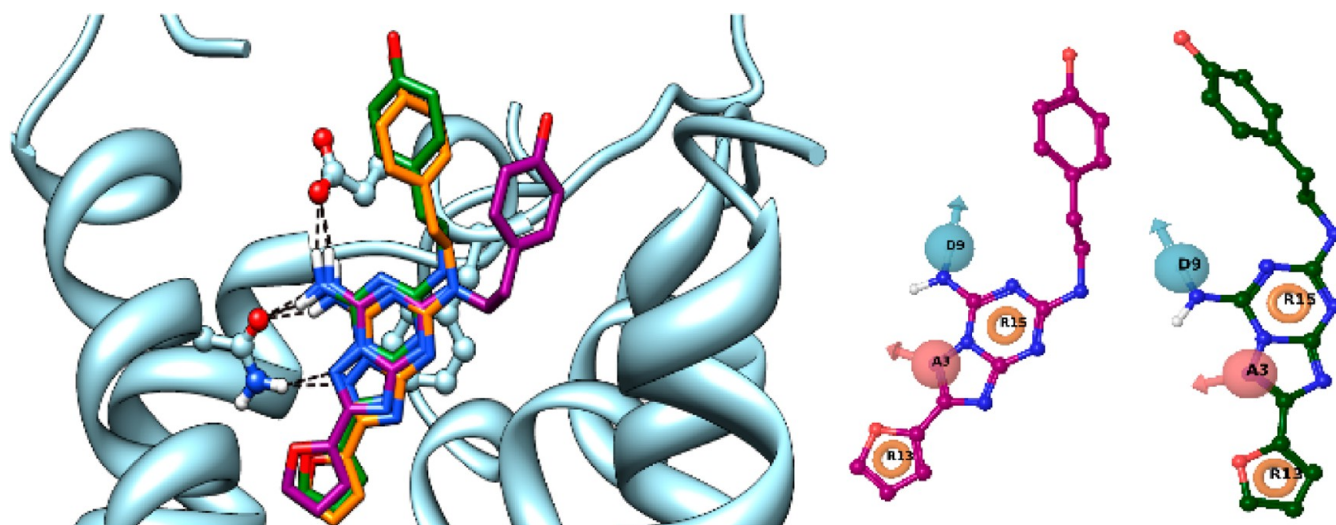


Figure 4. On the left: superposition of ZM 241385 *best pose* (dark magenta) and *selected pose* (green) conformations to the crystal pose of ZM 241385 (orange) in the binding pocket of the hA_{2A} AR. On the right: pharmacophore hypothesis for the *best pose* (dark magenta) and *selected pose* (green) protocol.

Table 2. Pharmacophore Based 3D-QSAR Model Results^a

pharmacophore based 3D-QSAR model	best pose database	selected pose database
training set	599 mol	599 mol
test set	149 mol	149 mol
PCs	6	7
r^2	0.49	0.55
q^2	0.42	0.44
RMSE	0.78	0.75
F	92.3	102
stability	0.93	0.94
calibration plot		
ROC plot		
threshold ROC	-2.78	-2.78
AUC	0.80	0.76
SE	0.04	0.05
correct predictions	712	714
incorrect predictions	36	34
Sensitivity	0.957	0.960
Specificity	0.888	0.888

^aPCs, principal components; r^2 , squared correlation coefficient of calibration (training set); q^2 , squared correlation coefficient of validation (test set); RMSE, root mean squared error; F, variance ratio (largest values correspond to better statistical significance); stability, stability of model predictions to changes in training set composition (max value 1); AUC, area under curve; SE, standard error of ROC curve; sensitivity and specificity are derived from the confusion matrices.

residues involved in hydrophobic contacts with most of the compounds, such as Val84 (3.32), Leu85 (3.33), Phe168 (EL2), Trp246 (6.48), Leu249 (6.51), and Ile274 (7.39). The most favorable hydrophobic interaction observed for all the compounds is mediated by Phe168 (EL2) through a π - π

stacking interaction with the heterocyclic aromatic core of the molecules.

In summary, the analysis of these maps has highlighted that the selected compounds, though possessing quite different chemical scaffolds, share a common binding mode at the hA_{2A} AR.

Table 3. Pharmacophore Based 3D-QSAR Model Predictions^a

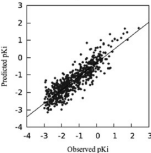
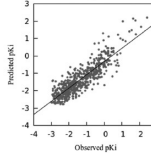
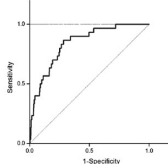
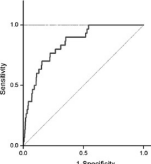
Pharmacophore-based 3D-QSAR model		mol	$pK_{i,obs}$	BP_{pred}	SP_{pred}	BP_{Fit}	SP_{Fit}
		1	-2.68	-1.71	-1.64	1.66	1.32
		2	-2.78	-1.81	-1.62	1.26	1.26
		3	-2.60	-1.84	-1.69	1.31	1.31
		4	-2.55	-1.71	-1.72	1.60	1.34
		5	-1.72	-1.79	-1.64	1.96	1.27
		6	-1.48	-1.98	-1.63	1.77	2.19
		7	-1.67	-1.54	-1.25	1.58	1.29
		8	-1.84	-1.62	-1.57	2.00	1.27
		9	-1.88	-1.66	-1.63	1.71	2.18
		10	-1.57	-1.67	-1.75	1.66	1.37
		11	-2.98	-1.76	-1.79	1.32	1.32
		12	-1.92	-1.85	-1.77	1.27	1.27
		13	-2.05	-2.20	-1.61	1.23	1.25
		14	-2.21	-1.65	-1.22	1.44	1.31
		15	-2.19	-1.12	-1.78	1.98	1.38
		16	-1.72	-1.67	-1.63	1.52	2.17
		17	-2.04	-1.52	-0.72	1.45	1.21
		18	-2.19	-1.62	-0.13	1.21	1.17
		19	-2.64	-1.49	-1.89	1.95	1.95
		20	-2.35	-1.71	-1.31	1.36	2.05
		21	-0.92	-1.80	-1.63	1.26	1.26
		22	-2.86	-1.71	-1.59	1.61	1.45
		23	-2.54	-1.97	-1.79	1.33	1.33
		24	-2.85	-1.94	-1.79	1.40	1.40
		25	-1.58	-1.78	-1.71	1.52	1.52
		26	-1.81	-1.73	-1.80	1.46	1.46
		27	-1.66	-1.74	-1.82	1.49	1.49
		28	-1.89	-0.36	-0.26	1.86	1.86
		29	-1.72	-1.97	-1.79	1.40	1.39

^aBP, best pose conformations; SP, selected pose conformations; Fit, fitness (it is a modified version of the survival score for hypothesis—it measures how well the molecules pharmacophore site points align to those of the hypothesis, how well the matching vector features (A,D,R) overlay those of the hypothesis, and how well the matching conformation superimposes, in an overall sense, with the reference ligand conformation); horizontal line ($pK_i = -2.78$) reports threshold active–inactive compounds.

The following step of our analysis has been the use of the docking conformations as input structures for the generation and selection of a common pharmacophore hypothesis. As described in the Materials and Methods section, the procedure

implemented in PHASE⁸⁵ suggests the consideration of only a subset of the active compounds: We initially attempted to consider only the most active molecule for each scaffold. This choice, however, did not lead to a common hypothesis unless it

Table 4. Atom Based 3D-QSAR Model Results^a

atom based 3D-QSAR model	best pose database	selected pose database
training set	601 mol	601 mol
test set	150mol	150 mol
PCs	6	5
r^2	0.78	0.76
q^2	0.58	0.51
RMSE	0.66	0.69
F	340.8	381.0
stability	0.853	0.924
calibration plot		
ROC plot		
threshold ROC	-2.78	-2.78
AUC	0.84	0.85
SE	0.04	0.04
correct predictions	718	720
incorrect predictions	33	31
Sensitivity	0.968	0.969
Specificity	0.888	0.920

^aPCs, principal components; r^2 , squared correlation coefficient of calibration (training set); q^2 , squared correlation coefficient of validation (test set); RMSE, root mean squared error; F , variance ratio (largest values correspond to better statistical significance); stability, stability of model predictions to changes in training set composition (max value 1); AUC, area under curve; SE, standard error of ROC curve; sensitivity and specificity are derived from the confusion matrixes.

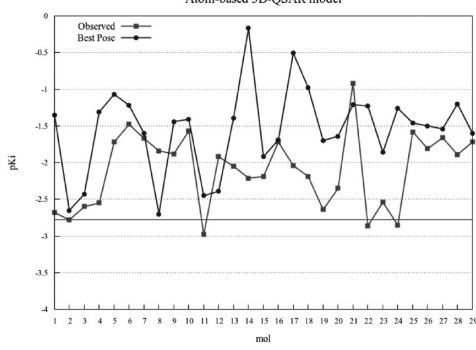
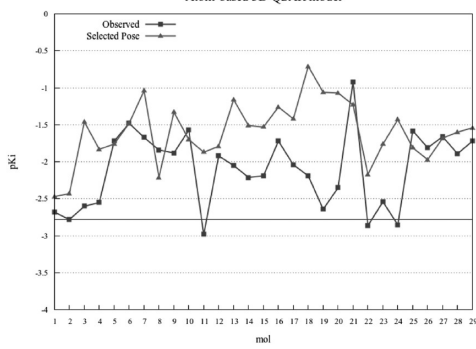
was after some of the scaffolds were removed, and the best model obtained with such a procedure had four PCs, a r^2 of 0.4, and q^2 of 0.3 (data not shown). Considering its statistical weakness, we decided not to further proceed with this approach and to use the crystal structure of ZM 241385 and its docked conformation as an active subset (at least two compounds are needed) to derive a common pharmacophore hypothesis consistent with all scaffolds. Through the procedure described in the Materials and Methods section, we obtained the following top score hypotheses: AADR, ADHR, ADHR, and ADDR. According to the most important interactions detected for the reference ligand ZM 241385 at the hA_{2A} AR, we have chosen the four-point ADHR hypothesis for the subsequent 3D-QSAR analysis.⁸⁹ Among the best 10% of surviving plausible hypotheses with these features, we have selected the pharmacophore model that reports a hydrogen bond donor (D) on the amino group at the N⁷ position of the bicyclic core, a hydrogen bond acceptor (A) on the N¹ of the triazolotriazine, and two aromatic features (R) on the triazine and furan ring, respectively (Figure 4).

Next, all the ligands belonging to both data sets were aligned to the selected pharmacophore: all compounds matched at least 2 features, except mol166, mol167, and mol169. Those compounds have been therefore left out, as their molecular structures fit only the D feature of the hypothesis.

Then, both *pharmacophore*- and *atom-based* 3D descriptors were computed (see Materials and Methods section), and the corresponding *pharmacophore-based* and *atom-based* 3D-QSAR

models were generated. The *pharmacophore-based* 3D-QSAR analysis has been carried out considering a final training set of 599 molecules (80% of database) and a test set of 149 molecules (20% of database), randomly selected. The PLS has been performed on the training and test sets to obtain the optimal number of principal components (PCs) for deriving the best statistical 3D-QSAR model to define relationships between pharmacophore molecular descriptors and hA_{2A} AR pK_i values. PLS statistical results are reported in Table 2. The models resulting from both databases present similar statistical values: though the model corresponding to the *selected pose* database has slightly higher correlation coefficients, F , and *stability* values, it has one principal component more with respect to the *best pose* model. As the computed correlation coefficients are not too high, we analyzed also the Receiver Operating Characteristic (ROC) plot for the databases by setting the activity threshold at 600 nM (pK_i = -2.78), with the aim of verifying if the models are able to discern active from inactive compounds. The threshold value was selected on the basis of a classification model developed in a previous paper.⁴⁷ In such a model, the compounds were classified into highly active ($K_i < 100$ nM), active ($100 < K_i < 250$), medium active ($250 < K_i < 500$), and weakly active ($K_i > 600$). We therefore decided to set the threshold to 600 nM to enable also medium and weakly active compounds to contribute to the definition of the pharmacophore models. The results of these analyses are reported in Table 2: In both cases, the area under curve (AUC) is around 0.8, and the curve line moves from the origin directly to good values of sensibility (ability to select actives) and specificity (ability to discard inactives). The ROC

Table 5. Atom Based 3D-QSAR Model Predictions^a

Atom-based 3D-QSAR model					
	mol	pKi obs	BPpred	SPpred	
	1	-2.68	-1.35	-2.47	
	2	-2.78	-2.65	-2.43	
	3	-2.60	-2.43	-1.46	
	4	-2.55	-1.31	-1.83	
	5	-1.72	-1.07	-1.76	
	6	-1.48	-1.22	-1.48	
	7	-1.67	-1.60	-1.04	
	8	-1.84	-2.70	-2.21	
	9	-1.88	-1.44	-1.33	
	10	-1.57	-1.41	-1.70	
	11	-2.98	-2.45	-1.87	
	12	-1.92	-2.39	-1.79	
	13	-2.05	-1.39	-1.16	
	14	-2.21	-0.17	-1.51	
Atom-based 3D-QSAR model					
	mol	15	-2.19	-1.92	-1.53
	16	-1.72	-1.69	-1.26	
	17	-2.04	-0.51	-1.42	
	18	-2.19	-0.98	-0.71	
	19	-2.64	-1.70	-1.06	
	20	-2.35	-1.64	-1.07	
	21	-0.92	-1.21	-1.23	
	22	-2.86	-1.23	-2.17	
	23	-2.54	-1.86	-1.76	
	24	-2.85	-1.26	-1.43	
	25	-1.58	-1.46	-1.81	
	26	-1.81	-1.50	-1.97	
	27	-1.66	-1.54	-1.68	
	28	-1.89	-1.20	-1.60	
	29	-1.72	-1.60	-1.54	

^aBP, best pose conformations; SP, selected pose conformations.

plots therefore suggest that these models can be used to qualitatively predict the activity of new compounds at the hA_{2A} AR.

With the aim to assess the ability of these two models to predict the activity of new antagonists, we have synthesized 29

pyrazolo-triazolo-pyrimidine (PTP) compounds. Indeed, our group has recently developed several series of PTP bearing different substitutions at the C², N⁵, and N⁸ positions, reported as promising hARs antagonists.^{50,95} Therefore, we have predicted

the pK_i values of these new derivatives, once molecular docking and pharmacophore feature generation have been performed on these structures.

Pharmacological characterization of the new compounds at the hA_{2A} AR has been carried out to compare the predicted values with the experimental outcomes. The results are reported in Table 3: In general, all the compounds fit the four pharmacophore features and in most of the cases, higher pK_i values are computed, thus implying that the compounds are predicted to be more active than experimentally determined. Only four compounds are predicted incorrectly (**2**, **11**, **22**, **24**): In fact, they exhibit experimental K_i values >600 nM ($pK_i = -2.78$) but are predicted as active molecules with K_i values <100 nM (see Table 3).

Apart from a few exceptions, both models are able to predict the activities in a range of 10–150 nM ($-2.17 < pK_i < -1$), therefore showing a good ability to select active compounds but a lower ability to discriminate between different structures and to discard the inactives. This can probably be ascribed to the fact that the good fitting of the four features of the common scaffold weights more than the diversity of the substituents, as we are considering *pharmacophore-based* descriptors.

We therefore also generated *atom-based* 3D-QSAR models for both the *best pose* and the *selected pose* data sets. The results of this analysis are reported in Table 4: The training set consists of 601 molecules and the test set, 150 molecules, and the correlation coefficients of both models are around 0.8. As far as the ability of the models to predict the K_i values of the 29 PTP compounds (external validation) is concerned, the correlation coefficients are 0.6/0.5 with six and five principal components for the *best pose* and the *selected pose* database, respectively.

Moreover, as for the *pharmacophore-based* ones, also for these models a further external validation has been conducted with the same set of 29 PTP.

Also in this case, four compounds (**2**, **11**, **22**, **24**) are incorrectly predicted as active (Table 5), while the corresponding experimental values are >600 nM ($pK_i = -2.78$). Moreover, the outliers are the same compounds that are incorrectly predicted by the *pharmacophore-based* 3D-QSAR model. A more careful inspection of their corresponding experimental values has revealed that the range of errors for all the molecules except compound **11** suggests that they can be considered also as active. Consequently, our predictions can be considered qualitatively reasonable also for these compounds. Another important aspect that emerges from the analysis of the *atom-based* 3D-QSAR model is that a focused range of predicted values cannot be identified as for the *pharmacophore based* model, thus implying that the predicted values are quantitatively more precise. It can be therefore concluded that the *atom-based* 3D-QSAR models are able to better correlate chemically diverse compounds with their activity. The higher accuracy of these results finds explanation in the better statistical parameters of *atom based* 3D-QSAR analysis, that, consequently, seems to be able to better correlate compounds of chemical diversity with activity.

CONCLUSIONS

In the present paper, we have investigated the SAR of hA_{2A} AR antagonists through an integrated *structure-* and *ligand-based* strategy. The availability of crystal structures of hA_{2A} AR bound to the antagonist ZM 241385 has allowed for the performance of molecular docking of a large database of hA_{2A} AR antagonists. Consequently, two databases have been collected: one with the best conformation for each antagonist selected by the docking

scoring function (*best pose* database), and one with the conformation that best reproduced the binding pattern observed in the crystallographic pose of ZM 241385 (*selected pose* database). For both sets, 3D-QSAR analyses with *pharmacophore-based* and *atom-based* molecular descriptors have been performed and validated. Our results suggest that the statistical quality of *atom-based* 3D-QSAR models enables quantitative discernment of active from inactive compounds, while *pharmacophore-based* 3D-QSAR models are limited to a qualitative prediction of the activity. Moreover, slightly better results can be obtained with the use of the *selected pose* database, even though no strong differences have been highlighted compared to the *best pose* database models, as the conformations of the two data sets often overlapped (for 546 molecules). As a consequence, we can conclude that, in this specific case under study, the best approach to predict hA_{2A} AR antagonists activity with this integrated strategy is to perform molecular docking and to use the *best pose* conformations as input for the *atom-based* 3D-QSAR analysis. This approach allows for time savings by avoiding the time-consuming visual inspection of docking poses as well as the computation and selection of pharmacophore hypotheses.

Considering that the applicability domain of pharmacophore-based screening approaches is more focused on the new hits identification rather than hit to lead optimization, our *best pose*—*atom based* 3D-QSAR model—can be used as a filtering tool for large chemical databases. This approach is currently in progress in our laboratory with the aim of scouting novel hA_{2A} AR antagonists within the MMsINC database.⁹⁹

ASSOCIATED CONTENT

Supporting Information

Complete training set, pharmacophore based 3D-QSAR model training and test set, and atom based 3D-QSAR model training and test set. This material is available free of charge via the Internet at <http://pubs.acs.org>.

AUTHOR INFORMATION

Corresponding Author

*Tel. +39 049 8275704. Fax +39 049 827 5366. E-mail: stefano.moro@unipd.it.

Author Contributions

These authors contributed equally to the work.

Notes

The authors declare no competing financial interest.

ACKNOWLEDGMENTS

The molecular modeling work coordinated by S.M. was carried out with financial support from the University of Padova, Italy, and the Italian Ministry for University and Research (MIUR), Rome, Italy. We are very grateful to Chemical Computing Group, Schrödinger and Molecular Networks for the long and fruitful collaborations.

ABBREVIATIONS

GPCRs, G Protein-Coupled Receptors; ARs, Adenosine Receptors; PTP, Pyrazolo-Triazolo-Pyrimidine; 3D-QSAR, 3D-Quantitative Structure-Activity Relationship

REFERENCES

(1) Fredholm, B. B.; Arslan, G.; Halldner, L.; Kull, B.; Schulte, G.; Wasserman, W. Structure and function of adenosine receptors and their genes. *Naunyn-Schmiedeberg's Arch. Pharmacol.* **2000**, *362*, 364–374.

- (2) Downey, J. M.; Cohen, M. V.; Ytrehus, K.; Liu, Y. Cellular mechanisms in ischemic preconditioning: the role of adenosine and protein kinase Ca. *Ann. N. Y. Acad. Sci.* **1994**, *723*, 82–98.
- (3) Auchampach, J. A.; Jin, X.; Wan, T. C.; Caughey, G. H.; Linden, J. Canine mast cell adenosine receptors: cloning and expression of the A₃ receptor and evidence that regranulation is mediated by the A_{2B} receptor. *Mol. Pharmacol.* **1997**, *52*, 846–860.
- (4) Fozard, J. R.; McCarthy, C. Adenosine receptor ligands as potential therapeutics in asthma. *Curr. Opin. Invest. Drugs* **2002**, *3*, 69–77.
- (5) Richardson, P. J.; Kase, H.; Jenner, P. G. Adenosine A_{2A} receptor antagonists as new agents for the treatment of Parkinson's disease. *Trends Pharmacol. Sci.* **1997**, *18*, 338–344.
- (6) Ribeiro, J. A.; Sebastiao, A. M.; de Mendonca, A. Adenosine receptors in the nervous system: pathophysiological implications. *Prog. Neurobiol.* **2002**, *68*, 377–392.
- (7) Yan, L.; Burbiel, J. C.; Maass, A.; Muller, C. E. Adenosine receptor agonists: from basic medicinal chemistry to clinical development. *Expert Opin. Emerging Drugs* **2003**, *8*, 537–576.
- (8) Fredholm, B. B. Adenosine receptors as targets for drug development. *Drug News Perspect.* **2003**, *16*, 283–289.
- (9) Moro, S.; Spalluto, G.; Jacobson, K. A. Techniques: Recent developments in computer-aided engineering of GPCR ligands using the human A₃ adenosine receptor as an example. *Trends Pharmacol. Sci.* **2005**, *26*, 44–51.
- (10) Fredholm, B. B.; Ijzerman, A. P.; Jacobson, K. A.; Klotz, K. N.; Linden, J. International Union of Pharmacology. XXV. Nomenclature and classification of adenosine receptors. *Pharmacol. Rev.* **2001**, *53*, 527–552.
- (11) Moro, S.; Gao, Z. G.; Jacobson, K. A.; Spalluto, G. Progress in the pursuit of therapeutic adenosine receptor antagonists. *Med. Res. Rev.* **2006**, *26*, 131–159.
- (12) Pinna, A.; Volpini, R.; Cristalli, G.; Morelli, M. New adenosine A_{2A} receptor antagonists: actions on Parkinson's disease models. *Eur. J. Pharmacol.* **2005**, *512*, 157–164.
- (13) Vu, C. B.; Pan, D.; Peng, B.; Kumaravel, G.; Phadke, D.; Engber, T.; Huang, C.; Reilly, J.; Tam, S.; Petter, R. C. Studies on adenosine A_{2A} receptor antagonists: comparison of three core heterocycles. *Bioorg. Med. Chem. Lett.* **2004**, *14*, 4831–4834.
- (14) Dowling, J. E.; Vessels, J. T.; Haque, S.; Chang, H. X.; van Vloten, K.; Kumaravel, G.; Engber, T. M.; Jin, X.; Phadke, D.; Wang, J.; Ayyub, E.; Petter, R. C. Synthesis of [1,2,4]triazolo[1,5-*a*]pyrazines as adenosine A_{2A} receptor antagonists. *Bioorg. Med. Chem. Lett.* **2005**, *15*, 4809–4813.
- (15) Gang, Y.; Haque, S.; Sha, L.; Kumaravel, G.; Wang, J.; Engber, T. M.; Whalley, E. T.; Conlon, P. R.; Chang, H.; Kiesman, W. F.; Petter, R. C. Synthesis of alkyne derivatives of novel triazolopyrazines as A_{2A} adenosine receptor antagonists. *Bioorg. Med. Chem. Lett.* **2005**, *15*, 511–515.
- (16) Vu, C. B.; Shields, P.; Peng, B.; Kumaravel, G.; Jin, X.; Phadke, D.; Wang, J.; Engber, T.; Ayyub, E.; Petter, R. C. Triamino derivatives of triazolo triazine and triazolopyrimidines as adenosine A_{2A} receptor antagonists. *Bioorg. Med. Chem. Lett.* **2004**, *14*, 4835–4838.
- (17) Peng, B.; Kumaravel, G.; Yao, G.; Sha, L.; Van Vlijmen, H.; Bohnert, T.; Huang, C.; Vu, C. B.; Ensinger, C. L.; Chang, H.; Engber, T. M.; Whalley, E.; Petter, R. C. Novel bicyclic piperazine derivatives of triazolotriazine and triazolopyrimidine as highly potent and selective adenosine A_{2A} receptor antagonists. *J. Med. Chem.* **2004**, *47*, 6218–6229.
- (18) Vu, C. B.; Pan, D.; Kumaravel, G.; Smits, G.; Jin, X.; Phadke, D.; Engber, T.; Huang, C.; Reilly, J.; Tam, S.; Grant, D.; Hetu, G.; Petter, R. C. Novel diamino derivatives of [1,2,4]triazolo[1,5-*a*][1,3,5]triazine as potent and selective adenosine A_{2A} receptor antagonists. *J. Med. Chem.* **2005**, *48*, 2009–2018.
- (19) González, M. P.; Terán, C.; Teijeira, M. Search for New Antagonist Ligands for Adenosine Receptors from QSAR Point of View. How Close Are We? *Med. Res. Rev.* **2008**, *3*, 329–371.
- (20) Diniz, C.; Borges, F.; Santana, L.; Uriarte, E.; Oliveira, J. M. A.; Gonçalves, J.; Fresco, P. Ligands and Therapeutic Perspectives of Adenosine A_{2A} Receptors. *Curr. Pharm. Des.* **2008**, *14*, 1698–1722.
- (21) Michielan, L.; Bolcato, C.; Federico, S.; Cacciari, B.; Bacilieri, M.; Klotz, K. N.; Kachler, S.; Pastorin, G.; Cardin, R.; Sperduti, A.; Spalluto, G.; Moro, S. Combining selectivity and affinity predictions using an integrated Support Vector Machine (SVM) approach: An alternative tool to discriminate between the human adenosine A_{2A} and A₃ receptor pyrazolo-triazolo-pyrimidine antagonists binding sites. *Bioorg. Med. Chem.* **2009**, *17*, 5259–5267.
- (22) Yuzlenko, O.; Drabczyńska, A.; Kieć-Kononowicz, K. Predictive 3D-Quantitative Structure-Activity Relationship for A₁ and A_{2A} Adenosine Receptor Ligands. *QSAR Comb. Sci.* **2009**, *28*, 1442–1454.
- (23) Lu, P.; Wei, X.; Zhang, R.; Yuan, Y.; Gong, Z. Prediction of the binding affinities of adenosine A_{2A} receptor antagonists based on the heuristic method and support vector machine. *Med. Chem. Res.* **2011**, *20*, 1220–1228.
- (24) Kim, J.; Wess, J.; van Rhee, M.; Schoneberg, T.; Jacobson, K. A. Site-directed mutagenesis identifies residues involved in ligand recognition in the human A_{2A} adenosine receptor. *J. Biol. Chem.* **1995**, *270*, 13987–13997.
- (25) Kim, S.-K.; Gao, Z.-G.; Van Rompaey, P.; Gross, A. S.; Chen, A.; Van Calenbergh, S.; Jacobson, K. A. Modeling the adenosine receptors: comparison of the binding domains of A_{2A} agonists and antagonists. *J. Med. Chem.* **2003**, *46*, 4847–4859.
- (26) Ivanov, A. A.; Palyulin, V. A.; Zefirov, N. S. Computer aided comparative analysis of the binding modes of the adenosine receptor agonists for all known subtypes of adenosine receptors. *J. Mol. Graphics Model.* **2007**, *25*, 740–754.
- (27) Michielan, L.; Bacilieri, M.; Schiesaro, A.; Bolcato, C.; Pastorin, G.; Spalluto, G.; Cacciari, B.; Klotz, K. N.; Kaseda, C.; Moro, S. Linear and non-linear 3D-QSAR approaches in tandem with ligand-based homology modeling as a computational strategy to depict pyrazolo-triazolo-pyrimidine antagonists binding site of the human adenosine A_{2A} receptor. *J. Chem. Inf. Model.* **2008**, *48*, 350–363.
- (28) Jaakola, V. P.; Griffith, M. T.; Hanson, M. A.; Cherezov, V.; Chien, E. Y. T.; Lane, J. R.; Ijzerman, A. P.; Stevens, R. C. The 2.6 angstrom crystal structure of a human A_{2A} adenosine receptor bound to an antagonist. *Science* **2008**, *322*, 1211–1217.
- (29) Xu, F.; Wu, H.; Katritch, V.; Han, G. W.; Cherezov, V.; Stevens, R. Structure of an Agonist-Bound Human A_{2A} Adenosine Receptor. *Science* **2011**, *332*, 322–327.
- (30) Lebon, G.; Warne, T.; Edwards, P. C.; Bennett, K.; Langmead, C. J.; Leslie, A. G. W.; Tate, C. G. Agonist-bound adenosine A_{2A} receptor structures reveal common features of GPCR activation. *Nature* **2011**, *474*, 521–525.
- (31) Dore, A. S.; Robertson, N.; Errey, J. C.; Ng, I.; Hollenstein, K.; Tehan, B.; Hurrell, E.; Bennett, K.; Congreve, M.; Magnani, F.; Tate, C. G.; Weir, M.; Marshall, F. H. Structure of the Adenosine A_{2A} Receptor in Complex with ZM241385 and the Xanthines XAC and Caffeine. *Structure* **2011**, *19*, 1283–1293.
- (32) Hino, T.; Arakawa, T.; Iwanari, H.; Yurugi-Kobayashi, T.; Ikeda-Suno, C.; Nakada-Nakura, Y.; Kusano-Arai, O.; Weyand, S.; Shimamura, T.; Nomura, N.; Cameron, A. D.; Kobayashi, T.; Hamakubo, T.; Iwata, S.; Murata, T. G-protein-coupled receptor inactivation by an allosteric inverse-agonist antibody. *Nature* **2012**, *482*, 237–240.
- (33) Congreve, M.; Andrews, S. P.; Dore, A. S.; Hollenstein, K.; Hurrell, E.; Langmead, C. J.; Mason, J. S.; Ng, I. W.; Tehan, B.; Zhukov, A.; Weir, M.; Marshall, F. H. Discovery of 1,2,4-Triazine Derivatives as Adenosine A_{2A} Antagonists using Structure Based Drug Design. *J. Med. Chem.* **2012**, *55*, 1898–1903.
- (34) Liu, W.; Chun, E.; Thompson, A. A.; Chubukov, P.; Xu, F.; Katritch, V.; Han, G. W.; Heitman, L. H.; Ijzerman, A. P.; Cherezov, V.; Stevens, R. C. Structural Basis for Allosteric Regulation of GPCRs by Sodium Ions. *Science* **2012**, *337*, 232–236.
- (35) Vilar, S.; Karpiak, J.; Costanzi, S. Ligand and Structure-Based Models for the Prediction of Ligand-Receptor Affinities and Virtual Screenings: Development and Application to the β 2-Adrenergic Receptor. *J. Comput. Chem.* **2010**, *31*, 707–720.
- (36) Bacilieri, M.; Varano, F.; Deflorian, F.; Marini, M.; Catarzi, D.; Colotta, V.; Filacchioni, G.; Galli, A.; Costagli, C.; Kaseda, C.; Moro, S. Tandem 3D-QSARs approach as a valuable tool to predict binding

affinity data: desing of new Gly/NMDA receptor antagonists as a key study. *J. Chem. Inf. Model.* **2007**, *47*, 1913–1922.

(37) Michielan, L.; Bacilieri, M.; Kaseda, C.; Moro, S. Prediction of the aqueous solvation free Energy of organic compounds by using autocorrelation of molecular electrostatic potential surface properties combined with response surface analysis. *Bioorg. Med. Chem.* **2008**, *16*, 5733–5742.

(38) Bacilieri, M.; Paoletta, S.; Basili, S.; Fanton, M.; Moro, S. A novel generalized 3D-QSAR model of camptothecin analogs. *Mol. Inf.* **2011**, *30*, 2–13.

(39) Dixon, S. T.; Smondyrev, A. M.; Knoll, E. H.; Rao, S. N.; Shaw, D. E.; Friesner, R. A. PHASE: a new engine for pharmacophore perception, 3D-QSAR model development, and 3D database screening: 1. Methodology and preliminary results. *J. Comput.-Aided Mol. Des.* **2006**, *20*, 647–671.

(40) Parenti, M. D.; Fioravanzo, E.; Mabilia, M.; Gallo, G.; Ciacci, A. Induced fit and pharmacophore generation approach applied to A2A adenosine receptor antagonists. *ARKIVOC*. **2006**, *viii*, 74–82.

(41) Baraldi, P. G.; Tabrizi, M. A.; Bovero, A.; Avitabile, B.; Preti, D.; Fruttarolo, F.; Romagnoli, R.; Varani, K.; Borea, P. A. Recent Developments in the Field of A2A and A3 Adenosine Receptor Antagonists. *Eur. J. Med. Chem.* **2003**, *38*, 367–382.

(42) Baraldi, P. G.; Cacciari, B.; Romagnoli, R.; Spalluto, G.; Moro, S.; Klotz, K. N.; Leung, E.; Varani, K.; Gessi, S.; Merighi, S.; Borea, P. A. Pyrazolo[4,3-*e*]1,2,4-triazolo[1,5-*c*]pyrimidine Derivatives as Highly Potent and Selective Human A3 Adenosine Receptor Antagonists: Influence of the Chain at the N8 Pyrazole Nitrogen. *J. Med. Chem.* **2000**, *43*, 4768–4780.

(43) Baraldi, P. G.; Cacciari, B.; Moro, S.; Spalluto, G.; Pastorin, G.; Da Ros, T.; Klotz, K. N.; Varani, K.; Gessi, S.; Borea, P. A. Synthesis, Biological Activity, and Molecular Modeling Investigation of New Pyrazolo[4,3-*e*]1,2,4-triazolo[1,5-*c*]pyrimidine Derivatives as Human A3 Adenosine Receptor Antagonists. *J. Med. Chem.* **2002**, *45*, 770–780.

(44) Baraldi, P. G.; Tabrizi, M. A.; Bovero, A.; Avitabile, B.; Preti, D.; Fruttarolo, F.; Romagnoli, R.; Varani, K.; Borea, P. A. Recent Developments in the Field of A2A and A3 Adenosine Receptor Antagonists. *Eur. J. Med. Chem.* **2003**, *38*, 367–382.

(45) Guba, W.; Nettekoven, M.; Pullmann, B.; Riemer, C.; Schmitt, S. Comparison of Inhibitory Activity of Isomeric Triazolopyridine Derivatives towards Adenosine Receptor Subtypes or Do Similar Structures Reveal Similar Bioactivities? *Bioorg. Med. Chem. Lett.* **2004**, *14*, 3307–3312.

(46) Baraldi, P. G.; Fruttarolo, F.; Tabrizi, M. A.; Preti, D.; Romagnoli, R.; El-Kashef, H.; Moorman, A.; Varani, K.; Gessi, S.; Merighi, S.; Borea, P. A. Design, Synthesis, and Biological Evaluation of C9- and C2-substituted Pyrazolo[4,3-*e*]1,2,4-triazolo[1,5-*c*]pyrimidines as New A2A and A3 Adenosine Receptors Antagonists. *J. Med. Chem.* **2003**, *46*, 1229–1241.

(47) Michielan, L.; Federico, S.; Terfloth, L.; Hristozov, D.; Cacciari, B.; Klotz, K. N.; Spalluto, G.; Gasteiger, J.; Moro, S. Exploring Potency and Selectivity Receptor Antagonist Profiles Using a Multilabel Classification Approach: The Human Adenosine Receptors as a Key Study. *J. Chem. Inf. Model.* **2009**, *49*, 2820–2836.

(48) Lenzi, O.; Colotta, V.; Catarzi, D.; Varano, F.; Filacchioni, G.; Martini, C.; Trincavelli, L.; Ciampi, O.; Varani, K.; Marighetti, F.; Morizzo, E.; Moro, S. 4-amido-2-aryl-1,2,4-triazolo[4,3-*a*]quinoxalin-1-ones as new potent and selective human A3 adenosine receptor antagonists. synthesis, pharmacological evaluation, and ligand-receptor modeling studies. *J. Med. Chem.* **2006**, *49*, 3916–3925.

(49) Cheong, S. L.; Dolzhenko, A.; Kachler, S.; Paoletta, S.; Federico, S.; Cacciari, B.; Dolzhenko, A.; Klotz, K. N.; Moro, S.; Spalluto, G.; Pastorin, G. The Significance of 2-Furyl Ring Substitution with a 2-(para-substituted) Aryl Group in a New Series of Pyrazolo-triazolopyrimidines as Potent and Highly Selective hA3 Adenosine Receptors Antagonists: New Insights into Structure–Affinity Relationship and Receptor–Antagonist Recognition. *J. Med. Chem.* **2010**, *53*, 3361–3375.

(50) Baraldi, P. G.; Cacciari, B.; Romagnoli, R.; Klotz, K. N.; Spalluto, G.; Varani, K.; Gessi, S.; Merighi, S.; Borea, P. A. Pyrazolo[4,3-*e*]1,2,4-Triazolo[1,5-*c*]Pyrimidine Derivatives as Adenosine Receptor Ligands:

A Starting Point for Searching A2B Adenosine Receptor Antagonists. *Drug Dev. Res.* **2001**, *53*, 225–235.

(51) Poucher, S. M.; Keddie, J. R.; Singh, P.; Stoggall, S. M.; caulkett, P. W. R.; Gones, G.; Collins, M. G. The in vitro pharmacology of ZM 241385, a potent, non-xanthine, A2a selective adenosine receptor antagonist. *Br. J. Pharmacol.* **1995**, *115*, 1096–1102.

(52) Cole, A. G.; Stauffer, T. M.; Rokosz, L. L.; Metzger, A.; dillard, L. W.; Zeng, W.; Henderson, I. Synthesis of 2-amino-5-benzoyl-4-(2-furyl)thiazoles as adenosine A2A receptor antagonists. *Bioorg. Med. Chem.* **2009**, *19*, 378–381.

(53) Carlsson, J.; Yoo, L.; Gao, Z. G.; Irwin, J. J.; Shoichet, B. K.; Jacobson, K. A. Structure-Based Discovery of A2A Adenosine Receptor Ligands. *J. Med. Chem.* **2010**, *53*, 3748–3755.

(54) Taliani, S.; La Motta, C.; Mugnaini, L.; Simorini, F.; Salemo, S.; Marini, A. M.; Da Settimo, F.; Cosconati, S.; Cosimelli, B.; Greco, G.; Limongelli, V.; Marinelli, L.; Novellino, E.; Ciampi, O.; Daniele, S.; Trincevelli, M. L.; Martini, C. Novel N2-Substituted Pyrazolo[3,4-*d*]pyrimidine Adenosine A3 Receptor Antagonists: Inhibition of A3-Mediated Human Glioblastoma Cell Proliferation. *J. Med. Chem.* **2010**, *53*, 3954–3963.

(55) Novellino, E.; Cosimelli, B.; Ehlaro, M.; Greco, G.; Iadanza, M.; Lavecchia, A.; Rimoli, M. G.; Sala, A.; Da Settimo, A.; Primofiore, G.; Da Settimo, F.; Taliani, S.; La Motta, C.; Klotz, K. N.; Tusciano, D.; Trincavelli, M. L.; Martini, C. 2-(Benzimidazol-2-yl)quinoxalines: A Novel Class of Selective Antagonists at Human A1 and A3 Adenosine Receptors Designed by 3D Database Searching. *J. Med. Chem.* **2005**, *48*, 8253–8260.

(56) Da Settimo, F.; Primofiore, G.; Taliani, S.; Marini, A. M.; La Motta, C.; Simorini, F.; Salemo, S.; Sergianni, V.; Tuccinardi, T.; Martinelli, A.; Cosimelli, B.; Greco, G.; Novellino, E. 5-Amino-2-phenyl[1,2,3]triazolo[1,2-*a*][1,2,4]benzotriazin-1-one: A Versatile Scaffold To Obtain Potent and Selective A3 Adenosine Receptor Antagonists. *J. Med. Chem.* **2007**, *50*, 5676–5684.

(57) Elzein, E.; Kalla, R.; Li, X.; Perry, T.; Parkhill, E.; Palle, V.; Varkhedkar, V.; Gimbel, A.; Zeng, D.; Lustig, D.; Leung, K.; Zablocki, J. Novel 1,3-dipropyl-8-(1-heteroaryl-methyl-1H-pyrazol-4-yl)-xanthine derivatives as high affinity and selective A2B adenosine receptor antagonists. *Bioorg. Med. Chem. Lett.* **2006**, *16*, 302–306.

(58) Camaioni, E.; Costanzi, S.; Vittori, S.; Volpini, R.; Klotz, K. N.; Cristalli, G. New Substituted 9-Alkylpurines as Adenosine Receptor Ligands. *Bioorg. Med. Chem.* **1998**, *6*, 523–533.

(59) Priego, E. M.; von Frijtag, D. K.; Ijzerman, J.; Camarasa, A. P.; Pérez-Pérez, M. J. Pyrido[2,1-*f*]purine-2,4-dione Derivatives as a Novel Class of Highly Potent Human A3 Adenosine Receptor Antagonists. *J. Med. Chem.* **2002**, *45*, 3337–3344.

(60) Priego, E. M.; Pérez-Pérez, M. J.; von Frijtag Drabbe Kuenzel, J.; De Vries, H.; Ijzerman, A. P.; Camarasa, M. J.; Martin-Santamaria, S. Selective Human Adenosine A3 Antagonists based on Pyrido[2,1-*f*]purine-2,4-diones: Novel Features of hA3 Antagonist Binding. *Chem. Med. Chem.* **2008**, *3*, 111–119.

(61) Fernández, F.; Caamaño, O.; Nieto, M. I.; López, C.; García-Mera, X.; Stefanachi, A.; Nicolotti, O.; Loza, M. I.; Brea, J.; Esteve, C.; Segarra, V.; Vidal, B.; Carotti, A. 1,3-Dialkyl-8-N-substituted benzyloxycarbonylamino-9-deazaxanthines as potent adenosine receptor ligands: Design, synthesis, structure–affinity and structure–selectivity relationships. *Bioorg. Med. Chem.* **2009**, *17*, 3618–3629.

(62) Gillespie, R. J.; Bamford, S. J.; Botting, R.; Comer, M.; Denny, S.; Gaur, S.; Griffin, M.; Jordan, A. M.; Knight, A. R.; Lerpiniere, J.; Leonardi, S.; Lightowler, S.; McAteer, S.; Merrett, A.; Misra, A.; Padfield, A.; Reece, M.; Saadi, M.; Selwood, D. L.; Stratton, G. C.; Surry, D.; Todd, R.; Tong, X.; Ruston, V.; Upton, R.; Weiss, S. M. Antagonists of the Human A2A Adenosine Receptor. 4. Design, Synthesis, and Preclinical Evaluation of 7-Aryltriazolo[4,5-*d*]pyrimidines. *J. Med. Chem.* **2009**, *52*, 33–47.

(63) Baraldi, P. G.; Bovero, A.; Fruttarolo, F.; Romagnoli, R.; Tabrizi, M. A.; Preti, D.; Varani, K.; Borea, P. A.; Moorman, A. R. New Strategies for the Synthesis of A3 Adenosine Receptor Antagonists. *Bioorg. Med. Chem.* **2003**, *11*, 1461–1469.

- (64) Luthra, P. M.; Mishra, C. B.; Jha, P. K.; Barodia, S. K. Synthesis of novel 7-imino-2-thioxo-3,7-dihydro-2H-thiazolo [4,5-d] pyrimidine derivatives as adenosine A_{2A} receptor antagonists. *Bioorg. Med. Chem. Lett.* **2010**, *20*, 1214–1218.
- (65) Mantri, M.; de Graaf, O.; van Veldhoven, J.; Göblyös, A.; von Frijtag Drabbe Kuenzel, J. K.; Mulder-Krieger, T.; Link, R.; de Vries, H.; Beukers, M. W.; Brussee, J.; Ijzerman, A. P. 2-Amino-6-furan-2-yl-4-substituted Nicotinonitriles as A_{2A} Adenosine Receptor Antagonists. *J. Med. Chem.* **2008**, *51*, 4449–4455.
- (66) Matasi, J. J.; Caldwell, J. P.; Hao, J.; Neustadt, B.; Arik, L.; Foster, K. J.; Lachowicz, J.; Tulshian, D. B. The discovery and synthesis of novel adenosine receptor (A_{2A}) antagonists. *Bioorg. Med. Chem. Lett.* **2005**, *15*, 1333–1336.
- (67) McGuinness, B. F.; Cole, A. G.; Dong, G.; Brescia, M. R.; Shao, Y.; Henderson, I.; Rokosz, L. L.; Stauffer, T. M.; Mannava, N.; Kimble, E. F.; Hicks, C.; White, N.; Wines, P. G.; Quadros, E. Discovery of 2-aminoimidazopyridine adenosine A_{2A} receptor antagonists. *Bioorg. Med. Chem. Lett.* **2010**, *20*, 6845–6849.
- (68) Mishra, C. B.; Barodia, S. K.; Prakash, A.; Kumar, J. B. S.; Luthra, P. M. Novel 8-(furan-2-yl)-3-substituted thiazolo [5,4-e][1,2,4] triazolo-[1,5-c] pyrimidine-2(3H)-thione derivatives as potential adenosine A_{2A} receptor antagonists. *Bioorg. Med. Chem.* **2010**, *18*, 2491–2500.
- (69) Moorjani, M.; Luo, Z.; Lin, E.; Vong, B. G.; Chen, Y.; Zhang, X.; Rueter, J. K.; Gross, R. S.; Lanier, M. C.; Tellew, J. E.; Williams, J. P.; Lechner, S. M.; Malany, S.; Santos, M.; Crespo, M. I.; Díaz, J. L.; Saunders, J.; Slee, D. H. 2,6-Diaryl-4-acylaminopyrimidines as potent and selective adenosine A_{2A} antagonists with improved solubility and metabolic stability. *Bioorg. Med. Chem. Lett.* **2008**, *18*, 5402–5405.
- (70) Neustadt, B. R.; Liu, H.; Hao, J.; Greenlee, W. J.; Stamford, A. W.; Foster, C.; Arik, L.; Lachowicz, J.; Zhang, H.; Bertorelli, R.; Fredduzzi, S.; Varty, G.; Cohen-Williams, M.; Nga, K. Potent and selective adenosine A_{2A} receptor antagonists: 1,2,4-Triazolo[1,5-c]pyrimidines. *Bioorg. Med. Chem. Lett.* **2009**, *19*, 967–971.
- (71) Neustadt, B. R.; Hao, J.; Lindo, N.; Greenlee, W. J.; Stamford, A. W.; Tulshian, D.; Ongini, E.; Hunter, J.; Monopoli, A.; Bertorelli, R.; Foster, C.; Arik, L.; Lachowicz, J.; Nga, K.; Fenga, K. I. Potent, selective, and orally active adenosine A_{2A} receptor antagonists: Arylpiperazine derivatives of pyrazolo[4,3-e]-1,2,4-triazolo[1,5-c]pyrimidines. *Bioorg. Med. Chem. Lett.* **2007**, *17*, 1376–1380.
- (72) Okamura, T.; Kurogi, Y.; Nishikawa, H.; Hashimoto, K.; Fujiwara, H.; Nagao, Y. 1,2,4-Triazolo[5,1-i]purine Derivatives as Highly Potent and Selective Human Adenosine A₃ Receptor Ligands. *J. Med. Chem.* **2002**, *45*, 3703–3708.
- (73) Kalla, R. V.; Elzein, E.; Perry, T.; Li, X.; Gimbel, A.; Yang, M.; Zengb, D.; Zablocki, J. Selective, high affinity A_{2B} adenosine receptor antagonists: N-1 monosubstituted 8-(pyrazol-4-yl)xanthenes. *Bioorg. Med. Chem.* **2008**, *18*, 1397–1401.
- (74) Shao, Y.; Cole, A. G.; Brescia, M. R.; Qin, L. Y.; Duo, J.; Stauffer, T. M.; Rokosz, L. L.; McGuinness, B. F.; Henderson, I. Synthesis and SAR studies of trisubstituted purinones as potent and selective adenosine A_{2A} receptor antagonists. *Bioorg. Med. Chem. Lett.* **2009**, *19*, 1399–1402.
- (75) Shah, U.; Boyle, C. D.; Chackalamannil, S.; Neustadt, B. R.; Lindo, N.; Greenlee, W. J.; Foster, C.; Arik, L.; Zhai, Y.; Ng, K.; Wang, S.; Monopoli, A.; Lachowicz, J. E. Biaryl and heteroaryl derivatives of SCH 58261 as potent and selective adenosine A_{2A} receptor antagonists. *Bioorg. Med. Chem.* **2008**, *18*, 4199–4203.
- (76) Shinkre, B. A.; Kumar, T. S.; Gao, Z. G.; Deflorian, F.; Jacobson, K. A.; Trenkle, W. C. Synthesis and evaluation of 1,2,4-triazolo[1,5-c]pyrimidine derivatives as A_{2A} receptor-selective antagonists. *Bioorg. Med. Chem.* **2010**, *20*, 5690–5694.
- (77) Weyler, S.; Fülle, F.; Diekmann, M.; Schumacher, B.; Hinz, S.; Klotz, K. N.; Müller, C. E. Improving Potency, Selectivity, and Water Solubility of Adenosine A₁ Receptor Antagonists: Xanthines Modified at Position 3 and Related Pyrimido[1,2,3-cd]purinediones. *Chem. Med. Chem.* **2006**, *1*, 891–902.
- (78) Stefanachi, A.; Nicolotti, O.; Leonetti, F.; Cellamare, S.; Campagna, F.; Loza, M. I.; Brea, J. M.; Mazza, F.; Gavuzzo, E.; Carotti, A. 1,3-Dialkyl-8-(hetero)aryl-9-OH-9-deazaxanthines as potent A_{2B} adenosine receptor antagonists: Design, synthesis, structure–affinity and structure–selectivity relationships. *Bioorg. Med. Chem.* **2008**, *16*, 9780–9789.
- (79) Gillespie, R. J.; Bamford, S. J.; Gaur, S.; Jordan, A. M.; Lerpiniere, J.; Mansell, H. L.; Stratton, G. C. Antagonists of the human A_{2A} receptor. Part 5: Highly bio-available pyrimidine-4-carboxamides. *Bioorg. Med. Chem.* **2009**, *19*, 2664–2667.
- (80) Zhang, X.; Tellew, J. E.; Luo, Z.; Moorjani, M.; Lin, E.; Lanier, M. C.; Chen, Y.; Williams, J. P.; Saunders, J.; Lechner, S. M.; Markison, S.; Joswig, T.; Petroski, R.; Piercey, J.; Kargo, W.; Malany, S.; Santos, M.; Gross, M. S.; Wen, J.; Jalali, K.; O'Brien, Z.; Stotz, C. E.; Crespo, M. I.; Díaz, J. L.; Slee, D. H. Lead Optimization of 4-Acetylamino-2-(3,5-dimethylpyrazol-1-yl)-6-pyridylpyrimidines as A_{2A} Adenosine Receptor Antagonists for the Treatment of Parkinson's Disease. *J. Med. Chem.* **2008**, *51*, 7099–7110.
- (81) Moro, S.; Bacilieri, M.; Ferrari, C.; Spalluto, G. Autocorrelation of molecular electrostatic potential surface properties combined with Partial Least Squares analysis as alternative attractive tool to generate Ligand-Based 3D-QSARs. *Curr. Drug Discovery Technol.* **2005**, *2*, 13–21.
- (82) Moro, S.; Bacilieri, M.; Cacciari, B.; Spalluto, S. Autocorrelation of molecular electrostatic potential surface properties combined with Partial Least Squares analysis as new strategy for the prediction of the activity of human A₃ adenosine receptor antagonists. *J. Med. Chem.* **2005**, *48*, 5698–5704.
- (83) GOLD suite, version 5.1; Cambridge Crystallographic Data Centre: Cambridge, U. K. <http://www.ccdc.cam.ac.uk>.
- (84) MOE (Molecular Operating Environment), version 2010.10; Chemical Computing Group Inc.: Montreal, Quebec, Canada. <http://www.chemcomp.com>.
- (85) Dixon, S. T.; Smondyrev, A. M.; Knoll, E. H.; Rao, S. N.; Shaw, D. E.; Friesner, R. A. PHASE: a new engine for pharmacophore perception, 3D-QSAR model development, and 3D database screening: 1. Methodology and preliminary results. *J. Comput. Aided Mol. Des.* **2006**, *20*, 647–671.
- (86) Schrödinger Suite 2011; Schrödinger, LLC: New York. <http://www.schrodinger.com>.
- (87) Floris, M.; Sabbadin, D.; Medda, R.; Bulfone, A.; Moro, S. Adenosiland: Walking through adenosine receptors landscape. *Eur. J. Med. Chem.* **2012**, *58*, 248–257.
- (88) Ballesteros, J. A.; Weinstein, H. Integrated methods for the construction of three dimensional models and computational probing of structure-function relationships in G-protein coupled receptors. *Methods Neurosci.* **1995**, *25*, 366–428.
- (89) Federico, S.; Paoletta, S.; Cheong, S. L.; Pastorin, G.; Cacciari, B.; Stragliotto, S.; Klotz, K. N.; Siegel, J.; Gao, Z. G.; Jacobson, K. A.; Moro, S.; Spalluto, G. Synthesis and Biological Evaluation of a New Series of 1,2,4-Triazolo[1,5-a]-1,3,5-triazines as Human A_{2A} Adenosine Receptor Antagonists with Improved Water Solubility. *J. Med. Chem.* **2011**, *54*, 877–889.
- (90) Halgren, T. A.; Myrphy, R. B.; Friesner, R. A.; Beard, H. S.; Frye, L. L.; Pollard, W. T. Glide: a new approach for rapid, accurate docking and scoring 1 methods and assessment of docking accuracy. *J. Med. Chem.* **2004**, *47*, 1739–1749.
- (91) Korb, O.; Stüttgen, T.; Exner, T. E. PLANTS: Application of Ant Colony Optimization to Structure-Based Drug Design. *Lect. Notes Comput. Sci.* **2006**, *4150*, 247–258.
- (92) Gaspar, A.; Reis, J.; Kachler, S.; Paoletta, S.; Uriarte, E.; Klotz, K. N.; Moro, S.; Borges, F. Discovery of novel A₃ adenosine receptor ligands based on chromone scaffold. *Biochem. Pharmacol.* **2012**, *84*, 21–29.
- (93) Kozma, E.; Kumar, T. S.; Federico, S.; Phan, K.; Balasubramanian, R.; Gao, Z.-G.; Paoletta, S.; Moro, S.; Spalluto, G.; Jacobson, K. A. Novel fluorescent antagonist as a molecular probe in A₃ adenosine receptor binding assays using flow cytometry. *Biochem. Pharmacol.* **2012**, *83*, 1552–1561.
- (94) Poli, D.; Catarzi, D.; Colotta, V.; Varano, F.; Filacchioni, G.; Daniele, S.; Trincavelli, L.; Martini, C.; Paoletta, S.; Moro, S. The identification of the 2-phenylphthalazin-1(2 H)-one scaffold as a new

decorable core skeleton for the design of potent and selective human A₃ adenosine receptor antagonists. *J. Med. Chem.* **2011**, *54*, 2102–2113.

(95) Cheong, S. L.; Dolzhenko, A. V.; Paoletta, S.; Lee, E. P.; Kachler, S.; Federico, S.; Klotz, K. N.; Dolzhenko, A. V.; Spalluto, G.; Moro, S.; Pastorin, G. Does the combination of optimal substitutions at the C²-, N⁵- and N⁸-positions of the pyrazolo-triazolo-pyrimidine scaffold guarantee selective modulation of the human A₃ adenosine receptors? *Bioorg. Med. Chem.* **2011**, *19*, 6120–6134.

(96) Pastorin, G.; Da Ros, T.; Spalluto, G.; Deflorian, F.; Moro, S.; Cacciari, B.; Baraldi, P. G.; Gessi, S.; Varani, K.; Borea, P. A. Pyrazolo[4,3-*e*]-1,2,4-triazolo[1,5-*c*]pyrimidine derivatives as adenosine receptor antagonists. Influence of the N5 substituent on the affinity at the human A₃ and A_{2B} adenosine receptor subtypes: a molecular modeling investigation. *J. Med. Chem.* **2003**, *46*, 4287–4296.

(97) Francis, J. E.; Cash, W. D.; Psychoyos, S.; Ghai, G.; Wenk, P.; Friedmann, R. C.; Atkins, C.; Warren, V.; Furness, P.; Hyun, J. L.; Stone, G. A.; Desai, M.; Williams, M. Structure-activity profile of a series of novel triazoloquinazoline adenosine antagonists. *J. Med. Chem.* **1988**, *31*, 1014–1020.

(98) Klotz, K. N.; Hessling, J.; Hegler, J.; Owman, C.; Kull, B.; Fredholm, B. B.; Lohse, M. J. Comparative pharmacology of human adenosine receptor subtypes-Characterization of stably transfected receptors in CHO cells. *Naunyn-Schmiedeberg's Arch. Pharmacol.* **1998**, *357*, 1–9.

(99) Masciocchi, J.; Frau, G.; Fanton, M.; Sturlese, M.; Floris, M.; Pireddu, L.; Palla, P.; Cedrati, F.; Rodriguez-Tomé, P.; Moro, S. MMsINC: a large-scale chemoinformatics database. *Nucleic Acids Res.* **2009**, *37*, (Database issue): D284–90. Database available at <http://mms.dsfarm.unipd.it/MMsINC.html>.